PCCP

Screening of Metal Complexes and Organic Solvents using COSMOSAC-LANL model to Enhance the Energy Density in Non-aqueous Redox Flow Cell: Insight to the Solubility

Journal:	*Physical Chemistry Chemical Physics*
Manuscript ID	CP-ART-06-2021-002591.R1
Article Type:	Paper
Date Submitted by the Author:	14-Aug-2021
Complete List of Authors:	Karmakar, Anwesa; Los Alamos National Laboratory, Theoretical Division Mukundan, Rangachary; Los Alamos National Laboratory, MPA-11 Yang, Ping; Los Alamos National Laboratory, Theoretical Division Batista, Enrique; Los Alamos National Laboratory, Theoretical Division

Screening of Metal Complexes and Organic Solvents using COSMOSAC-LANL model to Enhance the Energy Density in Non-aqueous Redox Flow Cell: Insight to the Solubility

Anwesa Karmakar*†, Rangachary Mukundan‡, Ping Yang*† and Enrique R. Batista*†

*†Theoretical Division, Los Alamos National Laboratory, Los Alamos 87545

‡MPA-11 Division, Los Alamos National Laboratory, Los Alamos 87545

Abstract

In this paper, we have proposed a first principle methodology to screen the transition metal complexes against a particular organic solvent and the organic solvents against a particular transition metal complex based on their solubility information without the knowledge of heat of fusion and melting temperature. The energy density of a non-aqueous redox flow cell directly depends on the solubility of the redox active species in the non-aqueous medium. We have used the "COSMOSAC-LANL" activity coefficient model (RSC. Adv., (2019), 18506-18526; Phys. Chem. Chem. Phys.,(2019), 19667-19685) which is based on first principle COSMO calculations where the microscopic information passes to the macroscopic world via a dielectric continuum solvation model followed by a post statistical thermodynamic treatment of the self-consistent properties of the solute particle to calculate the solubility. To model the activity coefficient at infinite dilution for the binary mixtures, a 3-suffix Margules (3sM) function is introduced for the quantitative estimation of the asymmetric interactions and, for the combinatorial term, the Staverman-Guggenheim (SG) form is used. The new activity coefficient model is separately called "LANL" activity coefficient model. The metal complex and the organic solvent have been treated as a simple binary mixture. The present model has been applied to a set of 14 different organic solvents and 16 different transition metal complexes. Using the new LANL activity coefficient model in combination with the ADF-COSMOSAC-2013 model, we have shown how one can improve the solubility of a transition metal complex in an organic solvent. We applied our model to screen 84 binary mixtures to predict the compatible pair of redox active species and organic solvent to increase the energy density. The solvation mechanism of the transition metal complexes in the organic solvents was obtained using the new model. The results have been compared with the experimental and theoretical results where they are available.

---

*E-mail: anwesa.karmakar@gmail.com; pyang@lanl.gov; erb@lanl.gov

1 Introduction

Transition metal complexes such as tris-acetylacetonate metal complexes are ubiquitous in chemical processes from the separation[1] of Uranium isotopes to redox active species in battery technology.[2–24] Very recently their uses in non-aqueous redox flow cell have been noticed to replace the use of aqueous Vanadium redox flow cell.[2–24] It is already known from various theoretical and experimental studies that the non-aqueous solvents (such as organic solvents, mixture of organic solvent and ionic liquid)[2,3] have small electrochemical potential. According to the report of Gong *et al.*[24], the use of non-aqueous solvent can offer a wide range of working temperature, high cell voltage and potentially high energy density. The working ability at low temperature is the biggest advantage to replace the aqueous redox flow cell by the non-aqueous redox flow cell. For all these reasons, both organic solvent and ionic liquid have been getting importance in this field as non-aqueous solvating medium.[2–24] For a successful redox flow cell compatible redox active species/solvent, redox active species/supporting electrolyte and solvent/supporting electrolyte combination are the most important thing. The main features taken into considerations are (i) high active species solubility, (ii) high supporting electrolyte solubility and (iii) high solution conductivity. Metal complex (active species) solubility (ΔG^{solv}) in the non-aqueous medium can be modeled using the molecular dynamics simulation via thermodynamic integration in DFT. However, these calculations are computationally expensive, time consuming, demands specific expertise and thus not suitable for large scale industrial applications. Solubility in such cases can be calculated using Scatchard-Hildebrand[25], Hansen[26] solubility parameters and COSMO-RS model[27–29] however further statistical physics needs to be developed for the metal complexes and non-aqueous solvents. No COSMO-RS/COSMOSAC[30,31] parameters for metal and hence for their complexes exist. Also the implementation to any of these models is incredibly difficult task to do. A more detail explanation on this issue related to those continuum solvation models has been given in the latter section of this manuscript. For the highly correlated transition metal complexes classical empirical models are not appropriate therefore, one needs to model their solubility from *ab initio* calculations.

We have already shown in our previous work[32–34] how one can predict a good trend of solubility of the redox active materials in ionic liquids without having any apriori knowledge of heat of fusion and melting temperature using the first-principle COSMOSAC-LANL model.[32–34] We were not only able to predict the solubility of a metal complex in different ionic liquids but also to predict the solvent for best redox active species solubility in them using this model. The reason behind the experimentally observed dual-solute[2,3] effect has been explained using the model. We have shown how one can predict the best ionic liquid for a particular metal complex solubility in them by using the knowledge of activity coefficient ($\gamma^{\infty}_{i/S}$) at infinite dilution of the solute species in a particular ionic liquid. However, for certain tris-acetylacetonate transition metal complexes such as $Fe(acac)_3$ and $V(acac)_3$ which have almost similar σ profile, the model fails to predict the solubility in acetonitrile.[14]

In the current study, we have shown an approach to improve the solubility prediction using the new "LANL" activity coefficient model (previously stated in Ref. 32 and 38) in combination with the ADF-COSMOSAC-2013 model.[31,35] This model was used to screen the transition metal complexes for a particular organic solvent and organic solvents for a particular metal complex. The "COSMOSAC-LANL" was used to propose a minimal model to predict the experimental solubility of a particular transition metal complex $V(acac)_3$ in 6 different organic solvents without the knowledge of heat of fusion and melting temperature. Later, the model was extended to predict the experimental solubility of $V(acac)_3$ in additional 8 different organic solvents. Similarly, we have proposed a methodology to screen the 16 different transition metal complexes in a particular organic solvent acetonitrile without the knowledge of heat of fusion and melting temperature. In order to do so, a screening scheme has been proposed based on the σ profile due to the hydrogen bonded segment (p_σ(HB-Tot)) of the metal complex and organic solvent. A linear regression model between the experimental solubility and p_σ(HB-Tot) has been proposed. Finally, we screen 84 binary mixtures of 14 different transition metal complexes and 6 different organic solvents with respect to each other based on the σ profile (p_σ(HB-Tot)) information of the redox active species and the organic solvent. A new solubility parameter (χ) has been defined. The solvation mechanism deals with the main interactions

present between the solute and solvent species responsible for the solubility and was not explained before from the microscopic point of view for the solubility of transition metal complexes in the organic solvents. The role of these important interactions such as the electrostatic, hydrogen bond and dispersion interactions in the solubility was explained using the new COSMOSAC-LANL model in the current study. In the work of Thompson *et al.* published in 2017[14], they proposed a non-linear regression model to predict the solubility of certain tris-acetyleacetonate metal complexes in acetonitrile solvent. But the molecular forces responsible for the solubility results were not explained by the authors from the microscopic point of view. Also, the authors proposed their model to screen certain transition metal complexes against a particular organic solvent acetonitrile, whereas in the present work a model has been proposed to screen the organic solvents against a particular metal complex and vice versa. Therefore, the current study has covered a wide range of metal complexes, organic solvents and their binary mixtures to propose a compatible pair of redox active species and solvent. The results have been compared with the experimental and theoretical results where they are available for the better understanding of the underlying principle of the solubility model presented in this study.

The manuscript has been divided in the following sections. In section 2, the details of solubility theory calculation have been discussed. The computational details have been discussed in section 3. The discussion on various thermodynamic properties of binary mixtures has been given in section 4. The solubility of metal complex in acetonitrile organic solvent has been discussed in section 5. Solubility of $V(acac)_3$ in different organic solvents and the relation between the solubilities and p_σ(HB-Tot) (sigmaprofile due to the hydrogen bonded segment) have been given in section 6. A brief conclusion has been provided in section 7.

2 COSMOSAC-LANL Model

To model the activity coefficient and other thermodynamical properties we have used the new model COSMOSAC-LANL[32,33,36–38] which is composed of the long range Staverman-Guggenheim[39,40] combinatorial interactions and short range asymmetric term. To model

the asymmetric term, we have used the 3-suffix Margules (3sM)[41,42] function which has been modeled using the ADF-COSMOSAC-2013[31,35] model. The new "LANL"[32,38] activity coefficient model is

$$\ln(\gamma_{\mathrm{i/S}}^{\mathrm{LANL}}) = \ln(\gamma_{\mathrm{i/S}}^{\mathrm{comb}}) + \ln(\gamma_{\mathrm{i/S}}^{\mathrm{asym}})\,, \tag{1}$$

where, $\ln(\gamma_{\mathrm{i/S}}^{\mathrm{asym}}) = \left(\Delta G_{\mathrm{i/S}}^{\mathrm{asym}} - \Delta G_{\mathrm{i/i}}^{\mathrm{asym}}\right)/RT$ is the difference between the asymmetric interactions in mixture (i/S) and pure state (i/i), which represents the solvation free energy change in terms of the solute and solvent interactions when a solute particle goes into a fixed position in solution from a fixed position in its ideal state. The expression for the activity coefficients for both species i and j present in the binary mixture solution is

$$\ln\gamma_{\mathrm{i}} = \frac{\alpha_{\mathrm{i}} x_{\mathrm{j}}^2 + \beta_{\mathrm{i}} x_{\mathrm{j}}^3}{RT} \tag{2}$$

$$\ln\gamma_{\mathrm{j}} = \frac{\alpha_{\mathrm{j}} x_{\mathrm{i}}^2 + \beta_{\mathrm{j}} x_{\mathrm{i}}^3}{RT}\,, \tag{3}$$

where x_i and x_j are the mole fraction of the solute and solvent molecules, respectively. γ_i and γ_j are the activity coefficients of the solute and solvent molecules, respectively. $\alpha_{\mathrm{i}} = (2A_{\mathrm{ji}} - A_{\mathrm{ij}})$, $\beta_{\mathrm{i}} = (2A_{\mathrm{ij}} - 2A_{\mathrm{ji}})$, $\alpha_{\mathrm{j}} = (2A_{\mathrm{ij}} - A_{\mathrm{ji}})$, and $\beta_{\mathrm{j}} = (2A_{\mathrm{ji}} - 2A_{\mathrm{ij}})$. At infinite dilution Eqs. 2 and 3 can be written as $\ln\gamma_{\mathrm{i/S}}^{\mathrm{asym}} = A/RT$, where A is equal to $RT\ln\gamma_{\mathrm{i/S}}^{\infty}$ and which is either A_{ij} (accounts solubility of species i in j) or A_{ji} (accounts solubility of species j in i). We use the activity coefficient at infinite dilution (γ^{∞}) calculated using ADF-COSMOSAC-2013[31] model to compute the Margules parameters for all binary mixture solutions. The same Staverman-Guggenheim (SG)[39,40] combinatorial term used in the work of Xiong *et al.*[31,43] has been used here

$$\ln(\gamma_{\mathrm{i/S}}^{\mathrm{comb}}) = 1 - \frac{\phi_{\mathrm{i}}}{x_{\mathrm{i}}} + \ln\frac{\phi_{\mathrm{i}}}{x_{\mathrm{i}}} - \frac{z}{2} q_{\mathrm{i}} \left(1 - \frac{\phi_{\mathrm{i}}}{\theta_{\mathrm{i}}} + \ln\frac{\phi_{\mathrm{i}}}{\theta_{\mathrm{i}}}\right), \tag{4}$$

with $\theta_{\mathrm{i}} = (x_{\mathrm{i}} q_{\mathrm{i}})/(\sum_{j=1}^{j=2} x_{\mathrm{j}} q_{\mathrm{j}})$ and $\phi_{\mathrm{i}} = (x_{\mathrm{i}} r_{\mathrm{i}})/(\sum_{j=1}^{j=2} x_{\mathrm{j}} r_{\mathrm{j}})$; r_{i} and q_{i} are the normalized volume and surface area parameters for species i and z is the coordination number equal to 10. This coordination number has been obtained by fitting the experimental data and the details are given in the work of Xiong *et al.*[31,43] The zq_{i} represents the number of nearest-neighbor sites to one of the solute and solvent molecules. In this model for

combinatorial term only the surface area q_i has been normalized with $q_0 = 79.53$ because r_0 will cancel out in the above equation. The details have been given in Appendix A. After adding the energy terms for combinatorial and asymmetric interactions described above, we obtain the expression for the activity coefficient for species i in solution S. Therefore, the expressions of the total activity coefficient for solute (i) and solvent (j) species are;

$$\ln\gamma_{\mathrm{i/S}}^{\mathrm{LANL}} = 1 - \frac{\phi_\mathrm{i}}{x_\mathrm{i}} + \ln\frac{\phi_\mathrm{i}}{x_\mathrm{i}} - \frac{z}{2}q_\mathrm{i}\left(1 - \frac{\phi_\mathrm{i}}{\theta_\mathrm{i}} + \ln\frac{\phi_\mathrm{i}}{\theta_\mathrm{i}}\right) + \frac{\alpha_\mathrm{i}x_\mathrm{j}^2 + \beta_\mathrm{i}x_\mathrm{j}^3}{RT}, \quad (5)$$

and

$$\ln\gamma_{\mathrm{j/S}}^{\mathrm{LANL}} = 1 - \frac{\phi_\mathrm{j}}{x_\mathrm{j}} + \ln\frac{\phi_\mathrm{j}}{x_\mathrm{j}} - \frac{z}{2}q_\mathrm{j}\left(1 - \frac{\phi_\mathrm{j}}{\theta_\mathrm{j}} + \ln\frac{\phi_\mathrm{j}}{\theta_\mathrm{j}}\right) + \frac{\alpha_\mathrm{j}x_\mathrm{i}^2 + \beta_\mathrm{j}x_\mathrm{i}^3}{RT}. \quad (6)$$

The Eqs. 5 and 6 are called as "LANL" activity coefficient model in the rest of the paper and in some cases the model is referred as COSMOSAC-LANL model as we imported Margules parameters from COSMOSAC-2013 model. At infinite dilution ($(x_{\mathrm{solute=i}} \longrightarrow 0\,, x_{\mathrm{solvent=j}} \longrightarrow 1$) the two models COSMOSAC-LANL and COSMOSAC-2013 are connected by

$$\ln\gamma_{\mathrm{i/S}}(\mathrm{COSMOSAC-LANL}) - \ln\gamma_{\mathrm{i/S}}(\mathrm{COSMOSAC-2013}) = \ln\gamma_{\mathrm{i/S}}(\mathrm{comb})\,. \quad (7)$$

The details of the derivation has been given in Appendix B. It is noteworthy in this regard that in the COSMOSAC-LANL model, the asymmetric interaction has been defined explicitly in terms of 3sM function and the residual interaction has been called implicitly within the 3sM function.[32,38] We calculated the total excess Gibbs free energy (G^{ex}) of the binary system from the equation

$$G^{\mathrm{ex}} = RT\left(x_\mathrm{i}\ln\gamma_{\mathrm{i/S}}^{\mathrm{COSMOSAC-LANL}} + x_\mathrm{j}\ln\gamma_{\mathrm{j/S}}^{\mathrm{COSMOSAC-LANL}}\right), \quad (8)$$

and the free energy of mixing for the binary mixture using

$$\Delta G^{\mathrm{mix}} = RT\left(x_\mathrm{i}\ln x_\mathrm{i} + x_\mathrm{j}\ln x_\mathrm{j} + x_\mathrm{i}\ln\gamma_{\mathrm{i/S}}^{\mathrm{COSMOSAC-LANL}} + x_\mathrm{j}\ln\gamma_{\mathrm{j/S}}^{\mathrm{COSMOSAC-LANL}}\right), \quad (9)$$

where x_i and x_j are the mole fractions of solute and solvent molecules in a binary mixture and $\ln\gamma_{\mathrm{i/S}}^{\mathrm{COSMOSAC-LANL}}$ and $\ln\gamma_{\mathrm{j/S}}^{\mathrm{COSMOSAC-LANL}}$ are the activity coefficients of solute and

solvent molecules, respectively obtained from the Eqs. 5 and 6. The solubility has been calculated[44] by

$$\ln x_{\mathrm{mc}} = -\ln\gamma_{\mathrm{mc}}(T,x) + \frac{\Delta H^{\mathrm{f}}_{\mathrm{mc}}(T_{\mathrm{m}})}{RT_{\mathrm{m}}}\left(1 - \frac{T_{\mathrm{m}}}{T}\right), \tag{10}$$

where, x_{mc} is the mole fraction of the metal complex in the liquid state, $\Delta H^{\mathrm{f}}_{\mathrm{mc}}$ is the heat of fusion and T_{m} is the melting temperature of the metal complex. For a particular metal complex ΔH_{mc} and T_{m} are fixed values, therefore, if we vary solvent, the solubility is a function of activity coefficient of the metal complex in liquid,

$$x_{\mathrm{mc}} \approx \frac{1}{\gamma_{\mathrm{mc}}}\,. \tag{11}$$

3 Computational details

Following the previous work,[32] all the COSMO[29] files for the metal complexes and organic solvents were generated using the Amsterdam Density Functional software.[31,45] The initial structures of each metal complexes and organic solvents have been drawn in ADFview or taken from the available crystal structures[1] for certain metal complexes. Then, they have been relaxed using a simple UFF method already implemented in ADF. After the UFF calculations, the geometry optimization was performed using generalized gradient approximation (GGA) with BP exchange correlation functional. The zeroth order regular approximation (ZORA) method was used for calculating the relativistic effect. TZP basis set for small frozen core and Becke integration with spline Zlm fit for density fitting have been used in ADF for each molecule followed by the post COSMOSAC calculation already implemented in ADF for the calculation of σ profile of each molecule. It is to be noted that the parameters used in the COSMOSAC-2013[31] model are not optimized for transition metals and hence for their complexes and not for all organic solvents. In COSMOSAC model, the electrostatic interaction is evaluated following the optimization of the molecular geometry, construction of the segmented surface, determination of segment properties such as the surface and screening charges. The screening charges on the solute nuclei interact with the solvent electron density (ρ) during the dissolution process by satisfying the criteria of minimum energy of solvation. The determination of the electrostatic interaction is composed of the energy difference between the molecule in the conductor and

vacuum and the energy difference between the molecule in the real solvent and conductor. The first interaction energy can be computed from the quantum COSMO calculation. This will lead to the COSMO-surface creation where COSMO radii have been determined by fitting COSMO predictions to the experimental data. Klamt optimized COSMO radii of 10 elements which can be found in Ref. 35. The COSMO radii for those 10 elements were optimized by using approximately 15000 DFT calculations. This COSMO radii have been used as default radii in all COSMOSAC models. Therefore, optimized COSMO radii is not present for the transition metal (V, Cr, Mn, Fe and Ru) in the current study. It is suggested by Klamt to use the COSMO radii 17% larger than the Pauli vDW radii in such cases and that requires the time consuming DFT optimization. In addition to this, the quantitative estimation of the restoring energy which is a function of the real solvent is done using statistical mechanics. According to the COSMOSAC model, the restoring energy is equivalent to the work required to add the additional segments on the surface of the solute to remove the screening charges. The self energy of a segment pair is the summation of the misfit, hydrogen bond and non bonded interaction (dispersion interaction). The misfit and hydrogen bond energy depend on the empirical parameters which can be obtained by fitting the experimental data. The details of the fitting procedure and the experimental data can be found in Ref. 31 for the COSMOSAC-2013 model for ADF software. At present, these parameters do not exist for the transition metals (V, Cr, Mn, Fe and Ru) and for the solvents (GBL, DMPU, MA, PC) used in this study due to the lack of required experimental data. The list of parameters which are not optimized for the above mentioned transition metals and the organic solvents are a_{eff}, r_{avg}, c_{es}, $c_{\text{OH-OH}}$, $c_{\text{OH-OT}}$, $c_{\text{OT-OT}}$, q_{s}, σ_0 and q_0. The details of the use of those parameters in the COSMOSAC model have been described in Refs. 31 and the references given in that article. Hence, in our calculations we used the parameters which were optimized for the simple organic solvents and their binary systems in the ADF software for COSMOSAC-2013 model. The unrestricted calculation considering spin polarization has been done only for the transition metal complexes as a new addition in the already stated COSMO setting in the work of Ref. 31. The details of the COSMO setting for the transition metal complexes and the organic solvents have been given in Table S-1 and S-2, respectively in the

supporting information. The charge and spin polarization need to be handled in case of the transition metal complexes in order to take into account the spin-orbit coupling in the transition metal complexes. This has been done with the key word CHARGE (NetQ (ab)) where the NetQ stands for the total charge of the metal complex and (ab) is the number of spin polarization. To account the spin polarization for these specific transition metal complexes, a non zero positive value has been used in the current study. The default spin polarization in ADF is zero which does not consider the spin polarization. The collinear approximation has been considered in the present study. In ADF, the spin-polarization has the same direction (default is in the direction of the z-axis) in each point in space in the collinear approximation where the Kramer's symmetry does not satisfied. Therefore, it is suggested to use the key word NOSYM for the spin symmetry. The transition metal complexes have been taken from the work of Ref. 14 and 46. 16 different transition metal complexes were categorized in four groups (i) Group I metal complexes: I, II, III, IV and V, in which the ligand is acetyleacetonate but the metal centre is different, (ii) Group II metal complexes: VI, VII, VIII, IX and X, in which the metal centre is Cr but the ligands are different and they are ester derivative of acetyleacetonate ligand (iii) Group III metal complexes: XI, XII and XIII, in which the metal centre is Cr but the ligands are different and they are -Br, -CN and -NO_2 derivative of acetyleacetonate ligand. (iv) Group IV metal complexes: XIV, XV and XVI, in which the metal centre is Cr and the ligand is -biphenyl derivative of acetyleacetonate ligand, respectively. The metal complexes have been shown in Figure. 1, 2 and 3. The metal complex X is different than the metal complex 14 in Ref. 14. However, X belongs to the same group of metal complexes 13 and 14 in Ref. 14. The COSMO points of certain metal complexes and 14 organic solvents have been shown in Figure. S-1-5 in the supporting information and in Figure. 2 and 3 in Ref. 32. For each COSMOSAC calculation, to ensure the minimization in optimized geometry, we also calculated the analytical frequency to check any presence of imaginary frequency in the calculated spectra for the organic solvents used in this study. The optimized geometry after this calculation has been used for the COSMOSAC calculation implemented in ADF for the COSMOSAC-2013 model.[31] The details of the quantum calculation setting for the analytical frequency calculations have been given in Table S-3.

The calculated analytical frequencies for the organic solvents for which we propose the solubility model have been given in Figure. S-6 of the supporting information. The all geometries are locally optimized for the transition metal complexes.

We computed σ profile for each transition metal complex and organic solvent using the ADF-COSMOSAC-2013 model.[31] σ profile is defined as the probability distribution for finding a segment of the COSMO surface with charge density σ and it is a unique property of a compound.[47] COSMOSAC[31,48] classifies the segment of the COSMO surface into three categories: (a) non hydrogen bonding, (b) hydrogen bonding from OH group and, (c) hydrogen bonding from other than OH group. A Gaussian like function has been considered to express the probability of hydrogen bonding segments (P^{HB})

$$P^{\mathrm{HB}} = 1 - \exp\left(-\frac{\sigma^2}{2{\sigma_0}^2}\right), \tag{12}$$

where σ is the screening charge density and σ_0 is equal to 0.007 e/Å^2 for the Gaussian distribution. The relation between them is $p_\sigma(HB) = p_\sigma(OH) + p_\sigma(OT)$ and thus $p_\sigma(Total) = p_\sigma(HB) + p_\sigma(NHB)$, where $p_\sigma(HB)$ is the σ profile due to the hydrogen bonded group, $p_\sigma(NHB)$ is profile due to the non-hydrogen bonded group and $p_\sigma(Total)$ is total σ profile. $p_\sigma(HB) = \frac{A_i^{HB}(\sigma)}{A_i} P^{\mathrm{HB}}(\sigma)$ and $p_\sigma(NHB) = \frac{A_i^{NHB}(\sigma)}{A_i} + \frac{A_i^{HB}(\sigma)}{A_i}[1 - P^{\mathrm{HB}}(\sigma)]$, where A_i is the COSMO surface. Here, $p_\sigma(OH)$ represents the σ profiles due to the hydrogen bonding surfaces ($A_i^{OH}(\sigma)$) on the hydroxyl (OH) group and $p_\sigma(OT)$ stands for the σ profiles due to the hydrogen bonding surfaces ($A_i^{OH}(\sigma)$) on the ketones, amine and nitro group other than hydroxyl (OH) group. The details of this COSMO partitioning based on the hydrogen-bonded segment information have been explained in Ref. 31 & 48. The final calculations for the thermodynamic properties have been done using the "LANL"[32] activity coefficient model. The COSMO volume, COSMO surface and σ profile of the pure compound are obtained from the ADF-COSMOSAC-2013 calculation.

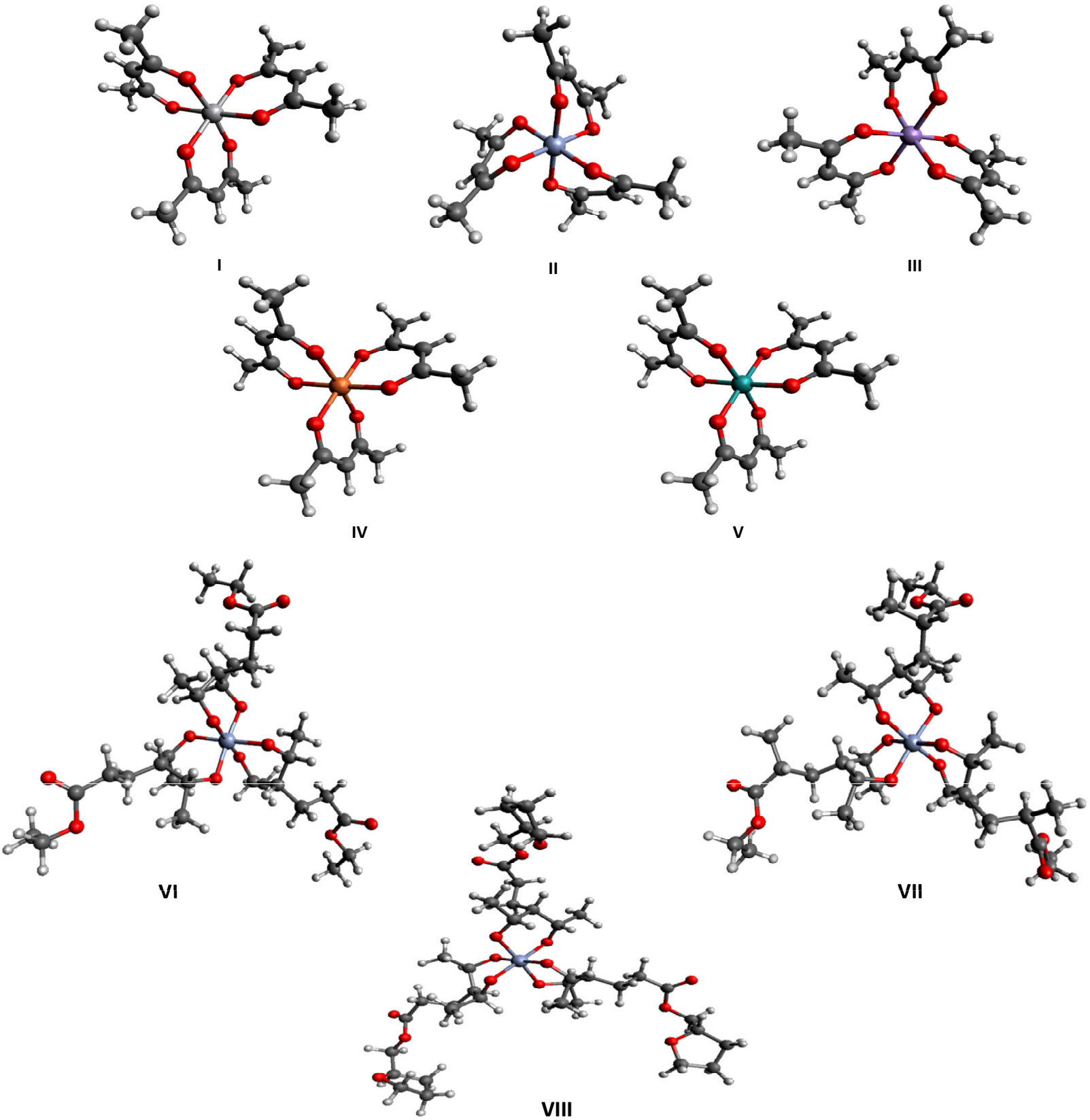

Figure 1: The different metal complexes. These complexes have been taken from the work of Thompson *et al.*[14,46]

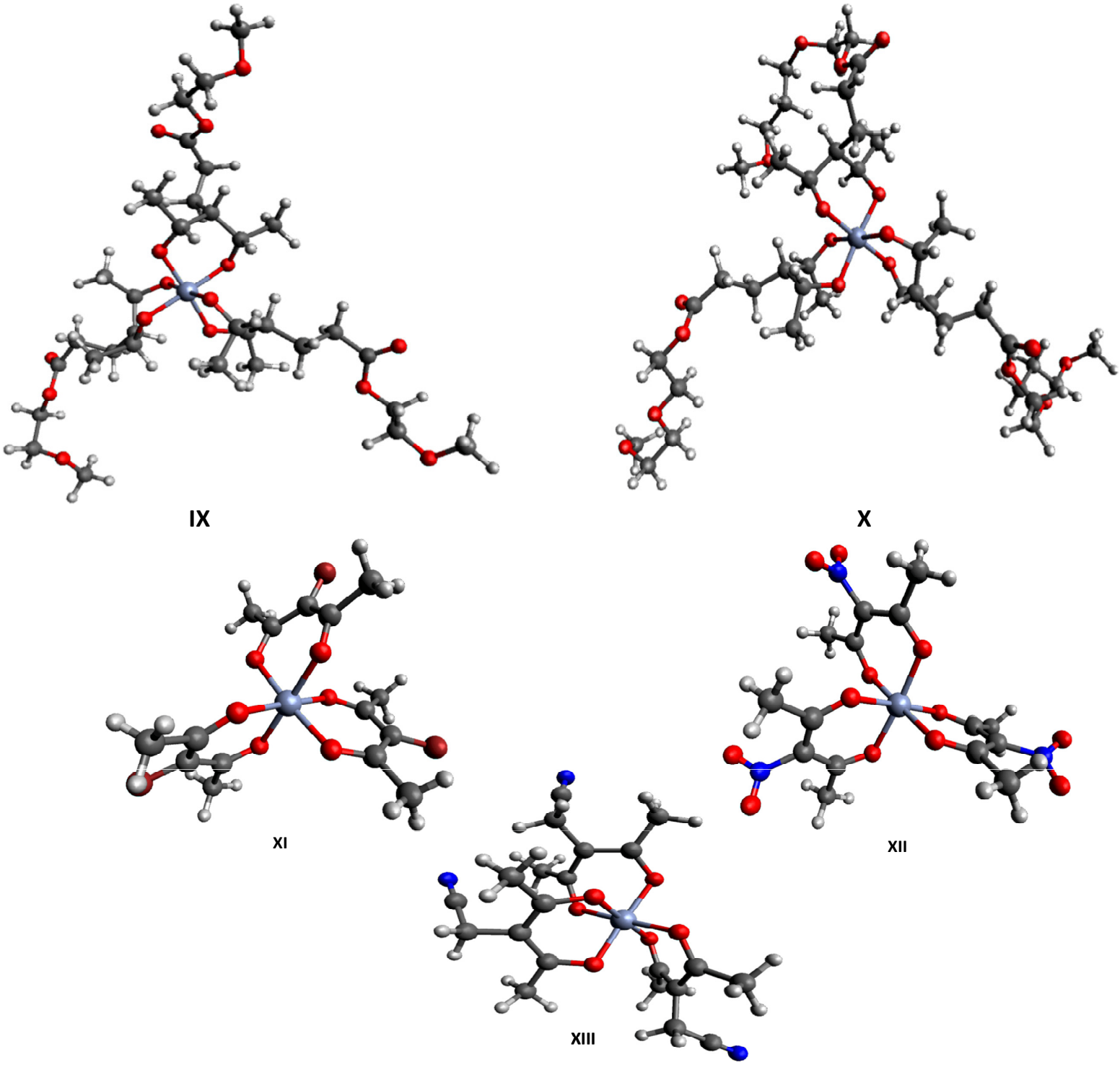

Figure 2: The different metal complexes. These complexes have been taken from the work of Thompson *et al.*[14,46]

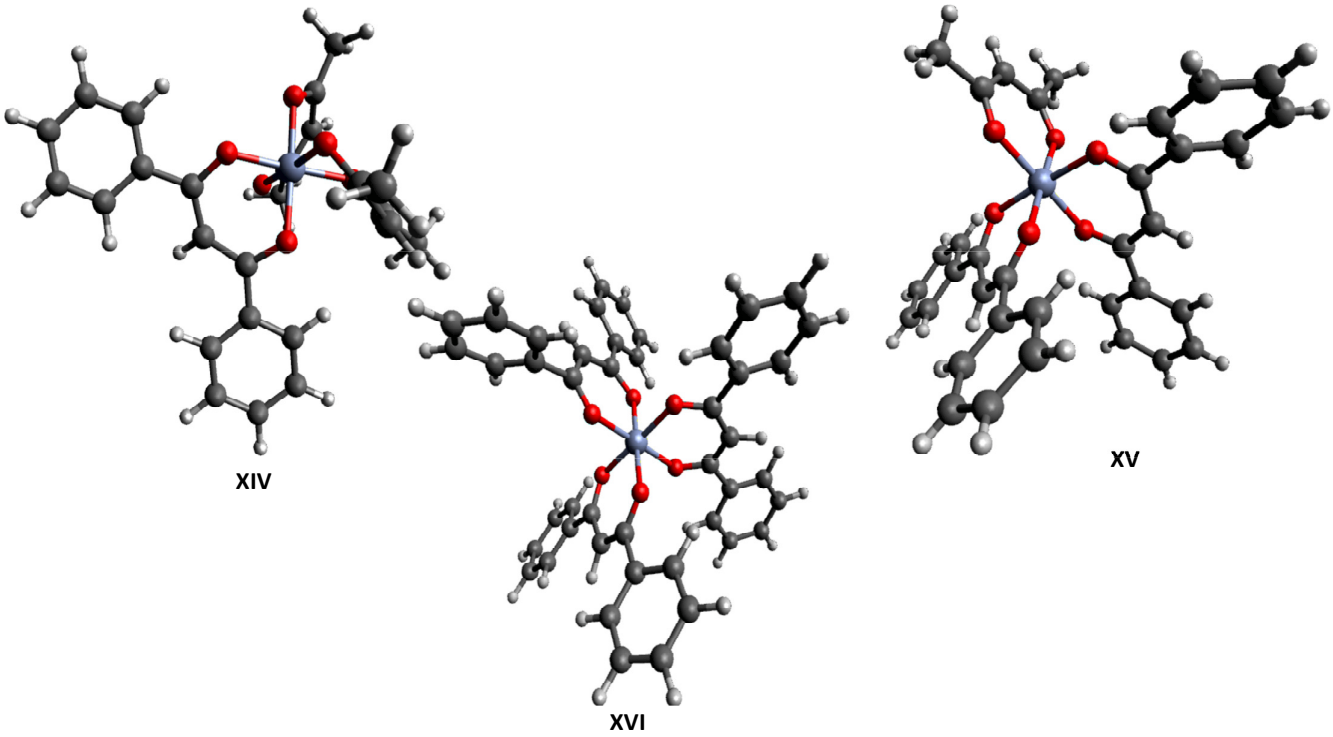

Figure 3: The different metal complexes. These complexes have been taken from the work of Thomson *et al.*[14,46]

4 Thermodynamic properties of binary mixtures

The asymmetric behavior of 13 different solutions comprising of transition metal complexes (I-XIII) in acetonitrile solvent have been shown in Figure. 4. The excess Gibbs free energy (G^{ex}) and Gibbs free energy of mixing (ΔG^{mix}) have been calculated for 13 different solutions and the results have been shown in the same figure. We have not included the results of transition metal complexes XIV, XV and XVI because their solubility in acetonitrile solvent is very low. We used these results to explain the experimental solubility results already reported in the work of Ref. 14. We use the different metal complexes belong to a particular group to present the results on G^{ex} and ΔG^{mix} and the correlations between $\ln\gamma_i$, $\ln\gamma_j$ and $\left(\ln\left(\frac{\gamma_{i/S}^{\text{LANL}}}{\gamma_{j/S}^{\text{LANL}}}\right)\right)$ with varying mole fraction (x_i) of solute species. According to the Eqs. 8, 9, 10 and 11, the calculated thermodynamic properties are function of the activity coefficient and of the individual metal complexes via their σ profiles. To account the effect of the systematic substitution in the acetylacetonate ligand on the solubility of the transition metal complexes, we decide to group the metal complexes and

that has been explained in computation section. In all three cases, we observed the excess Gibbs free energy shows minimum at mixture composition other than 50:50 composition of the binary solution and also the free energy curve does not symmetrically decay at the two ends. This asymmetric behavior of the excess free energy vs x_1 plot is in agreement with the asymmetric behavior of the model. To confirm this asymmetric behavior of the solution, we also plot the logarithm of the ratio of the activity coefficients $\left(\ln\left(\frac{\gamma_{i/S}^{\mathrm{LANL}}}{\gamma_{j/S}^{\mathrm{LANL}}}\right)\right)$ of solute and solvent molecule with variation of solute mole fraction x_i. The non linear curve in Figure. 4 is responsible for the asymmetric nature of the solution, which otherwise would be a straight line.[25] We also plot the logarithm of activity coefficient with mole fraction for both the solute and solvent species. The two curves intersect each other at a composition different from the 50:50 mixture composition in Figure. S-7-8. All these evidences for asymmetric interactions indicate towards the different type of complicated interactions present between the solute and solvent molecules in those solid-liquid equilibria during physical absorption of a particular transition metal complex in the organic solvent. The more asymmetric interaction observed for a solution indicates to the more deviation from the Raoult's Law. We have noticed that the binary mixture solutions showing maximum solubility of the metal complex in the organic solvent has widely varying asymmetric interaction in the solution and the trend decreases to the least soluble system for a particular group of metal complexes. This increasing asymmetric interaction is indicating to the more soluble metal complex in the organic solvent and which is satisfied by the maximum negative G^{ex} and ΔG^{mix} energy. Also, when we draw slopes for $\left(\ln\left(\frac{\gamma_{i/S}^{\mathrm{LANL}}}{\gamma_{j/S}^{\mathrm{LANL}}}\right)\right)$ of solute and solvent molecule with variation of solute mole fraction x_i for the metal complex II and X, we noticed the slopes in the respective curvatures for the metal complex X vary almost 2 times than that of the metal complex II. Such information confirms that the solute and solvent association is favorable and promote the solubility up to certain concentration limit and after that, the solute concentration decreases with increasing the solvent concentration. This variation in the slope is indicative to the supramolecular interactions present in those binary mixture and their variation with the concentration. These supramolecular interactions are the electrostatic, hydro-

gen bond and dispersion interaction present in those systems. Such variation of physical property with the concentration has been already reported in the work of Karmakar *et al.*.[49] They have shown in their work that such type of variation of a physical quantity with the species concentration is the consequence of the different supramolecular interactions present at the different concentration regime of a multi-component mixture solution using their first principle calculation. It is noticed from the study that the metal complexes having almost similar σ profile show almost similar G^{ex} and ΔG^{mix} for V(acac)$_3$ (I), Cr(acac)$_3$ (II), Mn(acac)$_3$ (III), Fe(acac)$_3$ (IV) and Ru(acac)$_3$ (V) metal complexes in Figure. 4 because the G^{ex} and ΔG^{mix} of those metal complexes are resulted from the COSMO surface of the different metal complexes shown in Figure. 4. The trend observed in the G^{ex} and ΔG^{mix} (X>IX>VIII>VII>VI) plot for the metal complexes VI-X of Group II agrees with the solubility trend (X>IX>VII>VIII>VI) reported in the work of Ref.14 and 46. For Group I, the experimental order of solubility is IV>III∼II∼I>V and the trend noticed in the G^{ex} and ΔG^{mix} is V>IV>III∼II∼I. The same for Group III metal complexes are XI>XII>XIII and XI>XIII>XII, respectively. We found that the systematic ester substitution in the acetylacetonate ligand affects the solubility of the transition metal complexes of Chromium. The metal complex with more negative G^{ex} and ΔG^{mix} is more soluble in acetonitrile solvent. Also, it is noteworthy that the stoichiometry of the solubility is found to change from 1:2 (x_{mc}∼0.5) complex to 1:3 (x_{mc}∼0.33) complex structure with increasing solubility of the metal complexes (II and VI - X) in Figure. 4(b) and (e). This also points to the enhancement in the solubility of the metal complex in acetonitrile solvent due to the present of electron donating group at the second position of the acetyleacetonate ligand which promote complexation interaction between the metal complex and the organic solvent. If one consider the two particular cases for II and X metal complexes and assume the metal complex as A and the solvent as B, the possible complex species are AB and AB$_2$ types, respectively. The second case for the metal complex (X) is indicative to the presence of a well defined 1:1 + 1:2 system according to the classical interpretation of Job Plot[50,51] which is a plot of intensive or extensive property vs the mole fraction of a species. The calculated Margules parameters have been given in Table. S-4 and S-5 in the supporting information. In order to find a qualitative rela-

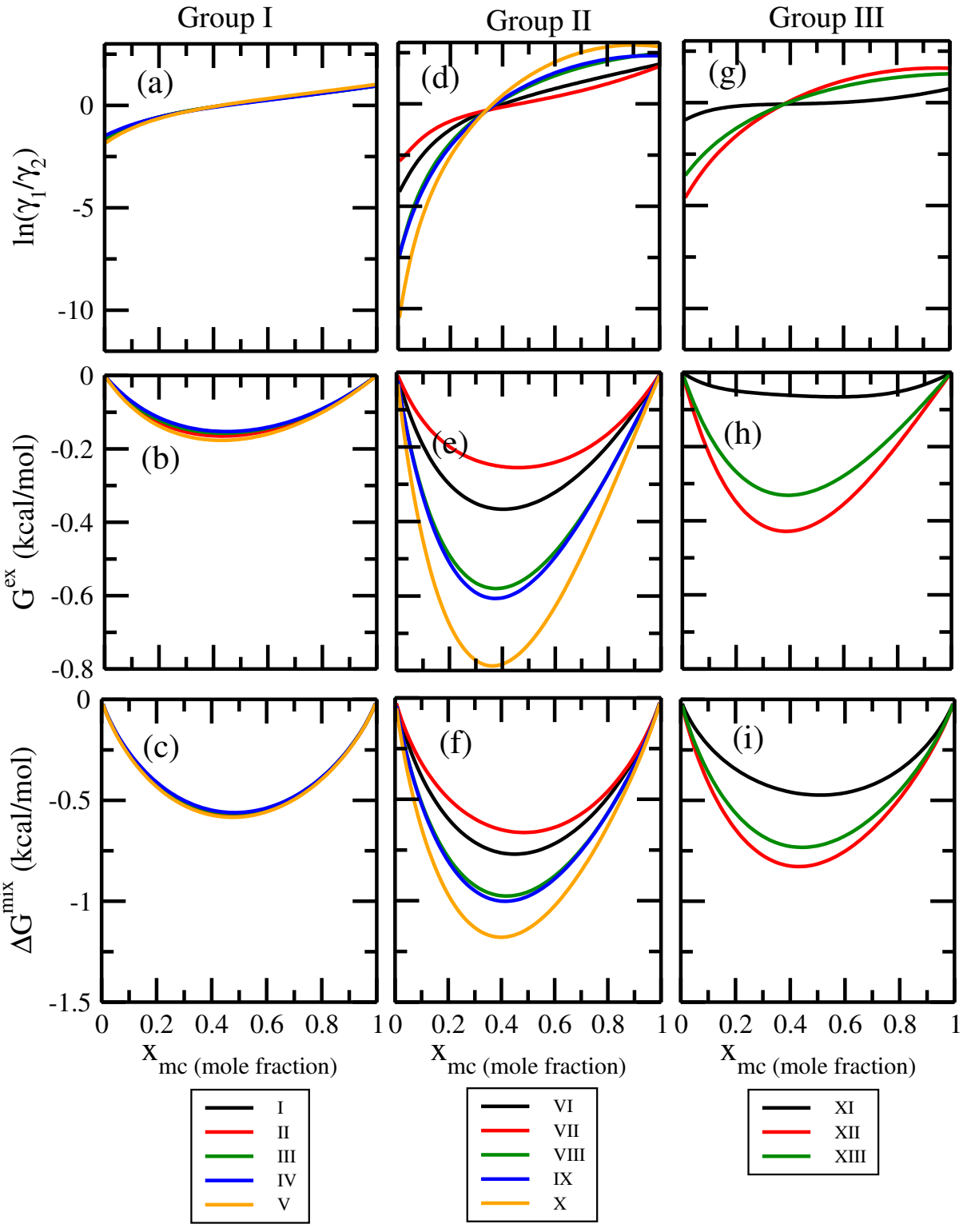

Figure 4: In fig (a), (d) and (g): $\ln\gamma_1/\gamma_2$, in fig (b), (e) and (h): G^{ex}, in fig (c), (f) and (i): ΔG^{mix} have been shown as a function of solute mole fraction for the metal complex. The γ_1 and γ_2 are the activity coefficient of the solute and solvent molecule, respectively. The solvent is acetonitrile (ACN).

tionship between the calculated G^{ex}, ΔG^{mix} and the σ profile of each metal complexes, we have also shown the σ profile of each metal complex in Figure. 5 and 6. We plotted the total σ profile due to all types of interactions (p_σ(Total)) and the σ profile due to the total hydrogen-bonded segment (p_σ(HB-Tot)) in Figure. 5 and 6. The p_σ(HB-Tot) of different metal complexes show significant differences in the σ profile for group I type of metal complexes. According to the present study the most soluble Fe(acac)$_3$ has more hydrogen-bonded segment than Ru(acac)$_3$ which is less soluble in ACN than Fe(acac)$_3$ shown in Figure. 5(b). This observation is in good agreement with the work of Ref. 14. The metal complexes belong to groups II, III and IV have significant differences in their thermodynamic properties and σ profile because group II, III and IV metal complexes have different ligands for a particular metal center and therefore, the ligand induced charge density on the metal center produces significant change in the σ profile of those systems. The COSMO surface point of certain metal complexes have been shown in Figure. S-1 and S-2 in the supporting information. We observed significant differences in p_σ(HB-Tot) in Figure. 5 and the same is observed in case of G^{ex} and ΔG^{mix} for group II and III types of metal complexes in Figure. 4. The results for the group IV metal complexes have been shown in Ref. 32. We noticed that the trend observed in the thermodynamic properties and σ profiles (in Figure. 4, 5 and 6) are well correlated with the trend noticed in the experimental solubility of those metal complexes in acetonitrile. Hence, we decided to correlate the particular p_σ(HB-Tot) with the experimental solubility of a metal complexes belong to group II, III and IV, i.e. the metal complexes with different type of ligands with same metal center to obtain a simplified solubility model for such systems. The details about the solubility modeling has been explained in the next section.

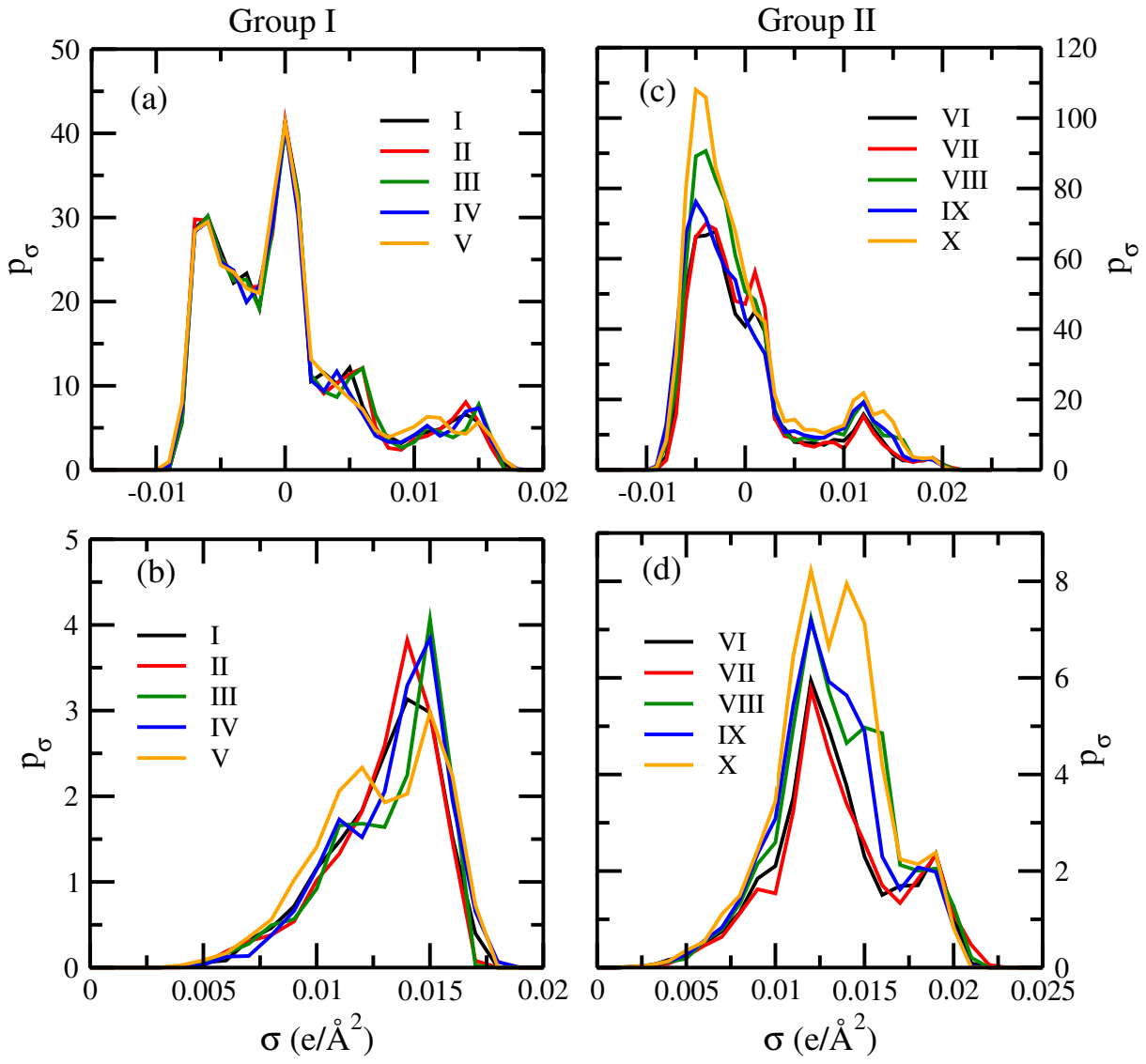

Figure 5: The total σ profile of group I and II metal complexes have been shown in (a) and (c), respectively. The corresponding p_σ(HB-Tot) has been shown in (b) and (d), respectively.

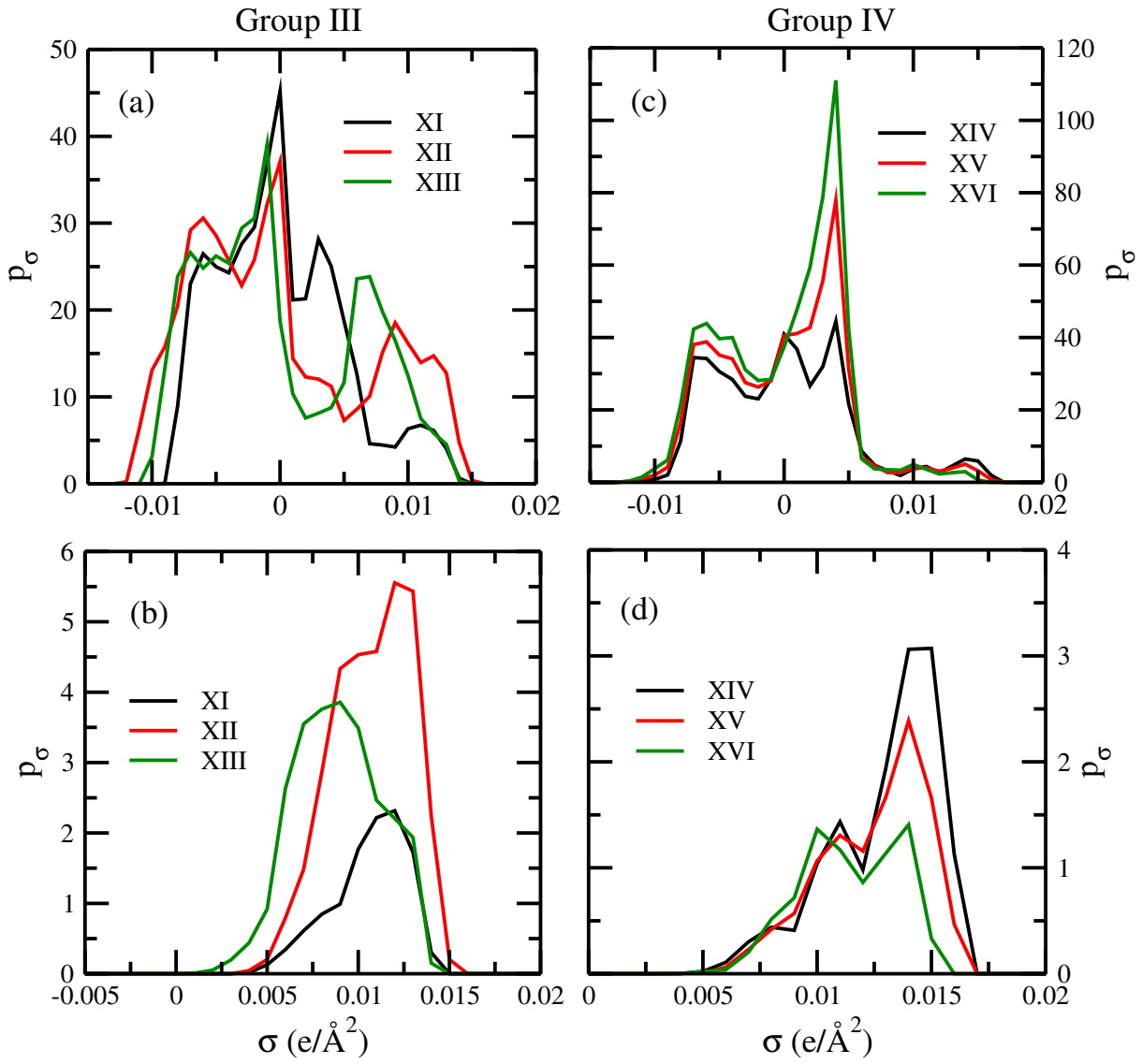

Figure 6: The total σ profile of group III and IV metal complexes have been shown in (a) and (c), respectively. The corresponding p_σ(HB-Tot) has been shown in (b) and (d), respectively.

5 Solubility of metal complexes in acetonitrile organic solvent

Solubility calculation of a transition metal complex in organic solvent needs (i) activity coefficient at infinite dilution ($\gamma^{\infty}_{i/S}$), (ii) heat of fusion and (iii) melting temperature according to Eq. 11. However, the last two informations are difficult to obtain. This restricts the application of the COSMOSAC model to screen the metal complexes for a particular organic solvent. The model can be used to screen the solvents for a particular metal complex. To propose the solubility model, we have differentiated two types of cases: (i) metal complexes with different metal center and same ligands and (ii) metal complexes with same metal center and different ligands, respectively. First we propose the model for the metal complexes with different metal center and same ligands. We have shown in the previous section that the metal complexes with different type of metal center with same ligands have almost similar type of σ profile and therefore have little variation in the G^{ex} and ΔG^{mix}. Almost similar type of COSMO surface and volume cannot be used to predict the solubility of those metal complexes because the solubility is a function of the activity coefficient, heat of fusion and melting temperature (see Eqs. 10 and 11). According to our study the Margules parameters and hence α_i, α_j, β_i and β_j are of the same order for the metal complexes of similar type of σ profile. Therefore, instead of correlating G^{ex} and ΔG^{mix} with the solubility we chose to correlate the experimental solubility and the calculated inverse of the activity coefficient at infinite dilution ($1/\gamma^{\infty}_{i/S}$) using the COSMOSAC-LANL model for group I type of metal complexes in acetonitrile solvent. We also showed the results for COSMOSAC-2013 model for same system. The results are shown in Figure. 7 and Table. 1. The correlation (coefficient of determination) between the experimental solubility and $1/\gamma^{\infty}_{i/S}$ is $\mathrm{R}^2 = 0.82$ for the COSMOSAC-LANL model, while the same is $\mathrm{R}^2 = 0.30$ for the COSMOSAC-2013 model. The better improvement in the first case is observed due to the correction included to the combinatorial term through the COSMOSAC-LANL model according to Eq. 7. This linear regression model is only valid for the metal complexes with similar type of ligands but with different metal center and can be easily used to screen group I type of metal complexes for a particular organic

solvent and to predict the right redox active species with better solubility in acetonitrile organic solvent.

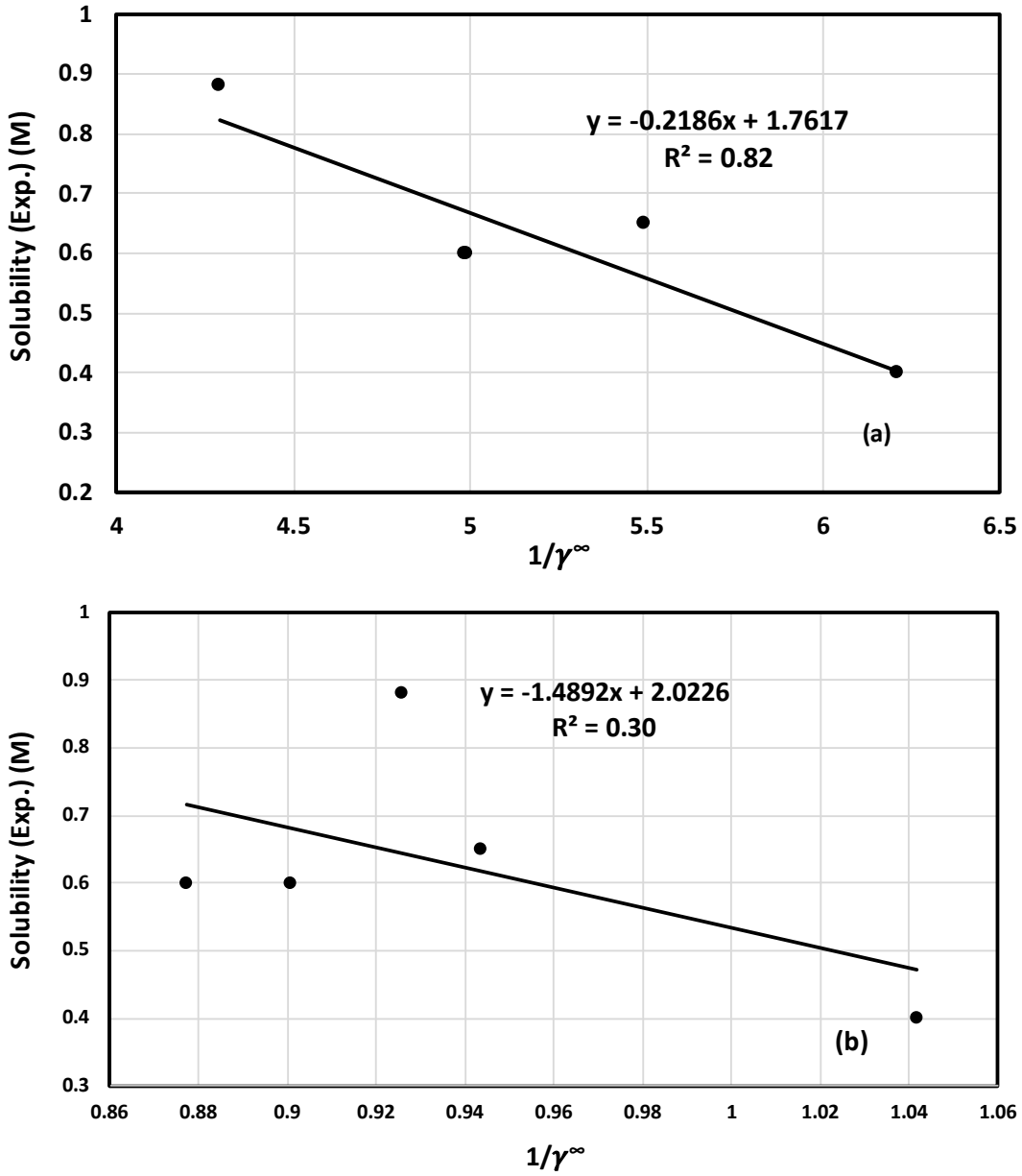

Figure 7: In fig. (a) and (b), the experimental solubility in molarity unit has been plotted as a function of $1/\gamma^{\infty}_{i/S}$ for the COSMOSAC-LANL and COSMOSAC-2013 model, respectively. These results have been shown for the metal complexes with different metal centers but same ligand.

In this paragraph, we proposed a new scheme to predict and screen the metal complexes with same metal center but different type of ligands. According to the discussion in

		$1/\gamma^{\infty}$		
Numbers	Metal Complex	COSMOSAC-2013	COSMOSAC-LANL	Solubility(Exp.)(M) [14,46]
1	$V(acac)_3$	0.88	4.99	0.60
2	$Cr(acac)_3$	0.94	5.49	0.65
3	$Mn(acac)_3$	0.90	4.99	0.60
4	$Fe(acac)_3$	0.93	4.29	0.88
5	$Ru(acac)_3$	1.04	6.21	0.40

Table 1: The experimental solubility (molarity) and calculated $1/\gamma^{\infty}_{i/S}$ of 5 different transition metal complexes in acetonitrile solvent.

section 4, we observed that the metal complexes with the same metal center but different ligands are significantly different from each other in terms of their solubility information such as G^{ex} and ΔG^{mix}. Unlike the metal complexes with different metal center, a good connection between the thermodynamic properties and the σ profile of the metal complexes has been observed for the metal complexes with different ligands and the same metal center (see Figure. 4, 5 and 6). For these cases, we correlated the experimental solubility with the p_σ(HB-Tot) and observe a good correlation between these two quantities shown in Figure. 8. The results are shown for II, VI-XVI metal complexes in a particular acetonitrile organic solvent in Figure. 8. When we removed the data point due to the XII and XIII metal complexes, the correlation coefficient improves from 0.82 for 12 to 0.90 for the 10 different metal complexes. According to the COSMOSAC-2013 model[31], the prediction power is not good for the nitrogen containing compound. Hence, we discard the results for XII and XIII metal complexes from our study. Also, we noticed that the experimental solubility of V and XI-XIV metal complexes is not good in comparison to the other transition metal complexes reported in Ref. 14. The experimental solubility of the metal complex X is not reported. Therefore, the experimental solubility has been taken in this study by following the simple relation: $x_X = \frac{p_\sigma(HB-Tot)_X}{p_\sigma(HB-Tot)_{IX}} * x_{IX}$. These two metal complexes are of similar type and they only vary at their alkoxy branching at the second position of the acetyleacetonate ligand. The calculated p_σ(HB-Tot) for 16 different metal complexes has been given in Table. 2. The different σ profiles of different metal complexes belong to different groups provide necessary information about the effect of the systematic

substitution of the acetylacetonate ligand on the metal complex solubility in acetonitrile organic solvent. The linear regression model can be used to predict the solubility of an unknown tris-acetylacetonate transition metal complex derivative in acetonitrile solvent with 82% precision and to design the new redox active species for a particular organic solvent acetonitrile in this case. We obtained a linear relationship between the experimen-

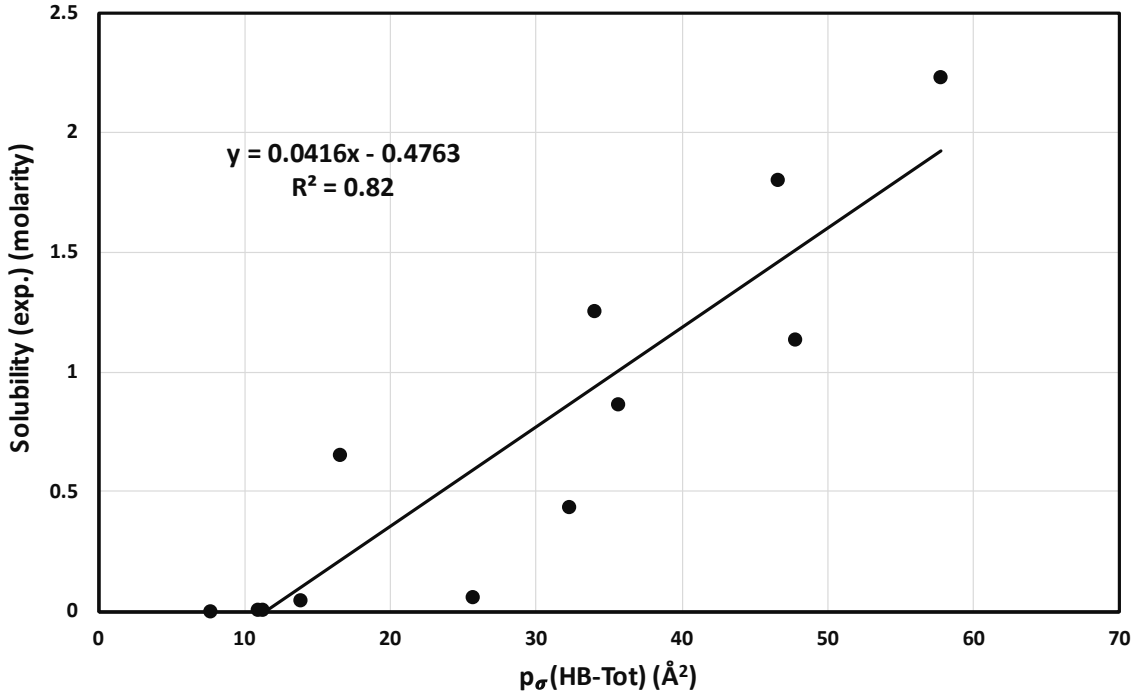

Figure 8: The experimental solubility in molarity unit as a function of p_σ(HB-Tot) for 12 different metal complexes. These results have been shown for the metal complexes with same metal center but different ligands.

tal solubility and the σ profile of particular type (p_σ(HB-Tot)). We found a correlation between these two properties with precision of 75%. The result has been shown in Figure. S-9(a)-9(b) in the supporting information. We notice that the precision between these two quantities increase from 75% to 85% when we remove the two outliers due to the points XII and XIII. Since the prediction power of the COSMOSAC-2013[31] model for the nitrogen containing compound is not good, we removed the results of metal complexes XII and XIII from our study. This has been shown in Figure. S-9(b) in the supporting information. All experimental solubilities reported for these 16 different transition metal complexes are measured in acetonitrile solvent in Refs. 14 and 46. Assuming constant

p_σ(HB-Tot) of acetonitrile solvent for all metal complexes, we propose that the solubility will be more between the solute and solvent species if the solute p_σ(HB-Tot) will be more for a particular organic solvent with less p_σ(HB-Tot). The experimental solubility depends on the activity coefficient at infinite dilution when a solute molecule is surrounded by large number of solvent molecules. Any solute molecule having more HB type of surfaces will like to form HB type of bond with the solvent molecule and dissolve in it, while the solvent molecule with more HB type surfaces will form HB type bond with themselves because they are present in large amount in the infinite dilute condition. Therefore, solute molecule with more HB type surface (electron donating/ electron accepting) would like to dissolve in solvent molecule having less HB type surface. When we removed the metal complexes XII, XIII and X from our calculation, we observed a correlation with precision $R^2 = 0.77$ which is very close to the solubility result in the Ref. 14. We removed metal complex X from our calculation because the experimental solubility of X was not reported in Ref. 14. The obtained results are in good agreement with the other experimental and theoretical results. We noticed that the reported correlation of determination is very near to that of Ref. 14. We calculated the error for both the models reported in this study and in Ref. 14 and they are 47.9% and 45.8%, respectively. The method of error calculation has been stated in section 1 in the supporting information. It is noteworthy in this regard that in the present study the correlation between the experimental solubility and the calculated p_σ(HB-Tot) has been reported to propose a minimal solubility model, while a correlation between the experimental and calculated solubility has been reported to validate the proposed solubility model in Ref. 14. Also, in the previous study reported in Ref. 14, the authors proposed a non-linear regression theoretical model to predict the experimental solubility. The solubility results are not explained from the microscopic point of view. In the present study, the solubility results have been explained from the microscopic point of view and a linear regression correlation model has been proposed between those microscopic property and the solubility. In addition to that, the previous model in Ref. 14 was proposed only for a selected metal complexes and a particular organic solvent ACN, while the present study is applicable for a wide range of metal complexes, organic solvents and their possible binary mixtures. The present model was also able to give a

physical insight to the theoretical model, the experimental solubility results and to predict a new possible binary mixture. Therefore, the two coefficients of determination(R^2) have different physical background in the two models. Also, the parameters in the solubility model in Ref. 14 are optimized while the parameters in COSMOSAC-LANL model are not optimized for the metal complex and organic solvent. Therefore, it is to be noted that this correlation can be improved more (>77%) when the COSMOSAC-LANL model will have the optimized parameters for the metal complex and the organic solvent. The model reported in this study is a simple solubility model based on the knowledge of a single property (p_σ(HB-Tot)) for the metal complexes with different type of ligands with the same metal center (i.e., II and VI-XIV) and same ligands with different metal center (i.e., I-V) and the organic solvents. Apart from the correlation between the experimental solubility and (p_σ(HB-Tot)) for all metal complexes, we propose a correlation between the experimental solubility and the activity coefficient at infinite dilution ($1/\gamma^{\infty}_{i/S}$) for the metal complexes with same ligands but different metal center. Also using the current model we explain the underlying principle behind the solubility of certain transition metal complexes in certain non-aqueous medium based on the quantitative-structure property relationship and on a single descriptor (p_σ(HB-Tot)) information which came out as a main governing factor for the solubility of certain metal complexes in certain non-aqueous solvents in the current study.

Complex	Solubility(Exp.)(M)[14,46]	p_σ(HB-Tot)(Å^2)	p_σ(Total)(Å^2)	%p_σ(HB-Tot)
I	0.60	16.64	357.69	4.652
II	0.65	16.56	357.32	4.635
III	0.60	15.94	353.29	4.512
IV	0.88	17.92	351.10	5.104
V	0.40	17.61	362.22	4.862
VI	0.86	35.65	637.70	5.590
VII	1.25	34.00	657.92	5.167
VIII	1.13	47.82	798.82	5.986
IX	1.8	46.61	728.61	6.397
X	>1.8	57.76	921.52	6.267
XI	0.002	11.27	411.09	2.741
XII	0.055	25.66	421.89	6.082
XIII	0.43	32.27	460.10	7.014
XIV	0.043	13.93	468.12	2.975
XV	8.00E-04	10.99	581.58	1.889
XVI	6.00E-05	7.76	697.31	1.113

Table 2: The p_σ(HB-Tot) and p_σ(Total) of 16 different metal complexes.

6 Solubility of V(acac)$_3$ in different organic solvents

We propose a scheme to screen the solvents with high solubility ($1/\gamma^{\infty}_{i/S}$) for a particular metal complex such as V(acac)$_3$ for which experimental results were available.[4] To propose the solvent screening for a particular transition metal complex, first we propose a model for limited 6 training data points for which the experimental solubility[4] of that metal complex is present. The transition metal complex V(acac)$_3$ has been used in this case. The solubility of V(acac)$_3$ in 6 different organic solvents has been given in Table. 3. We correlated the activity coefficient at infinite dilution for a particular metal complex with the experimental solubility reported in molarity unit for both the COSMOSAC-2013 and COSMOSAC-LANL model. The results have been shown in Table. 3. A very good correlation of $R^2 = 0.98$ is obtained for the COSMOSAC-LANL activity coefficient model in contrast with $R^2 = 0.23$ for COSMOSAC-2013 model. The results in the molarity unit have been shown in Figure. S-10(a) and 10(b). To calculate the percentage error in solubility, we convert the experimental solubility data from molarity unit to mole fraction using the relation given in next few lines. We know that the total mole fraction of the

system will be constant and therefore, $x_{\mathrm{V(acac)_3}} + x_{\mathrm{solvent}} = 1$, where $x_{\mathrm{V(acac)_3}}$ is the mole fraction of the V(acac)$_3$ and x_{solvent} is the mole fraction of the organic solvent. Now we know; $x_{\mathrm{solvent}} = \frac{m_{\mathrm{ACN}}}{M_{\mathrm{tot}}} = \frac{M_{\mathrm{solvent}}/\mathrm{Molar\ Mass_{solvent}}}{M_{\mathrm{tot}}(?)}$, where M_{solvent} is mole number of the solvent and M_{tot} is the total mole number of the binary mixture. Since $\rho = \frac{M_{\mathrm{solvent}}}{V_{\mathrm{sol}}}$, therefore, $x_{\mathrm{V(acac)_3}} = \frac{m_{\mathrm{V(acac)_3}}}{M_{\mathrm{tot}}}$. The density of 6 solvents has been given in Table. 3. The solubility result in mole fraction unit has been given in Table. 3 and 4 and the corresponding plot has been shown in Figure. 9. In the case of ideal solvation γ_{mc} =1 according to Eq. 11, the percentage error in the solubility is 28.2% and 70% for COSMOSAC-LANL and COSMOSAC-2013 model, respectively. This calculation has been done using Eq. 10. The ideal solvation has been calculated at the heat of fusion 7.17 kcal/mol[52] and melting temperature 460 K[52,53] for V(acac)$_3$ metal complex. The observed correlation coefficients (R^2) for the two models are 0.88 for COSMOSAC-LANL and 0.57 for COSMOSAC-2013, respectively in the mole fraction unit. We also compared the calculated solubility with the experimental solubility reported in mole fraction unit for the both models. The calculated % error in the linear regression is 10.86% and 90% for the COSMOSAC-LANL in Figure. 10(a) and COSMOSAC-2013 model in Figure. 10(b), respectively. The root mean square error (RMSE) value for the two models is shown in Table. 4 and they are 0.013 for COSMOSAC-LANL and 0.017 for COSMOSAC-2013 model, respectively. After verifying the predictive power and accuracy of the model, we use the COSMOSAC-LANL model to screen the organic solvents for the best solubility of V(acac)$_3$. In the set of 14 different solvents, the 6 solvents from the training data set are also included. The other 8 organic solvents have been chosen randomly. It is to be noted that the experimental solubility of V(acac)$_3$ in those 8 organic solvents has not yet been reported. The result has been shown in Figure. 11. The calculated solubility and the activity coefficient at infinite dilution have been correlated for the 14 different organic solvents with $R^2 = 0.98$ and the calculated % error in the linear regression is 26.72% at the ideal solvation $\gamma_{\mathrm{mc}} = 1$. Among 14 organic solvents, 1,3-dioxolane (1,3do) is appeared to be the most suitable solvent for the solubility of V(acac)$_3$ and this result is in good agreement with the experimental results reported in Ref. 5. Figure. 12 shows the $\ln\gamma_1/\gamma_2$ *vs* x_{mc}, G^{ex} *vs* $x_{\mathrm{mc}}$and ΔG^{mix} *vs* x_{mc} for 6 different organic solvents. The new model was able to explain

	$1/\gamma^{\infty}$		molarity	mole fraction	g cm^{-3}
Solvents	COSMOSAC-2013	COSMOSAC-LANL	Solubility(Exp.)[4]	Solubility(Exp.)	Density
PC	0.58	1.12	0.07	0.006	1.20
GBL	1.44	3.25	0.30	0.022	1.13
DMPU	1.89	2.65	0.20	0.024	1.06
ACN	0.88	4.98	0.60	0.03	0.786
MA	1.86	4.22	0.40	0.031	0.932
1,3do	2.27	6.62	0.80	0.064	1.06

Table 3: The experimental solubility (molarity), calculated solubility (mole fraction) and $1/\gamma^{\infty}_{i/S}$ of V(acac)$_3$ in 6 different organic solvents and density of 6 different organic solvents.

	mole fraction		mole fraction
Solvents	COSMOSAC-2013	COSMOSAC-LANL	Solubility(Exp.)
PC	0.008	0.015	0.006
GBL	0.019	0.038	0.022
DMPU	0.024	0.033	0.024
ACN	0.013	0.049	0.03
MA	0.024	0.047	0.031
1,3do	0.028	0.062	0.064
RMSE	0.017	0.013	-

Table 4: The experimental and calculated solubility of V(acac)$_3$ in 6 different organic solvents in mole fraction unit.

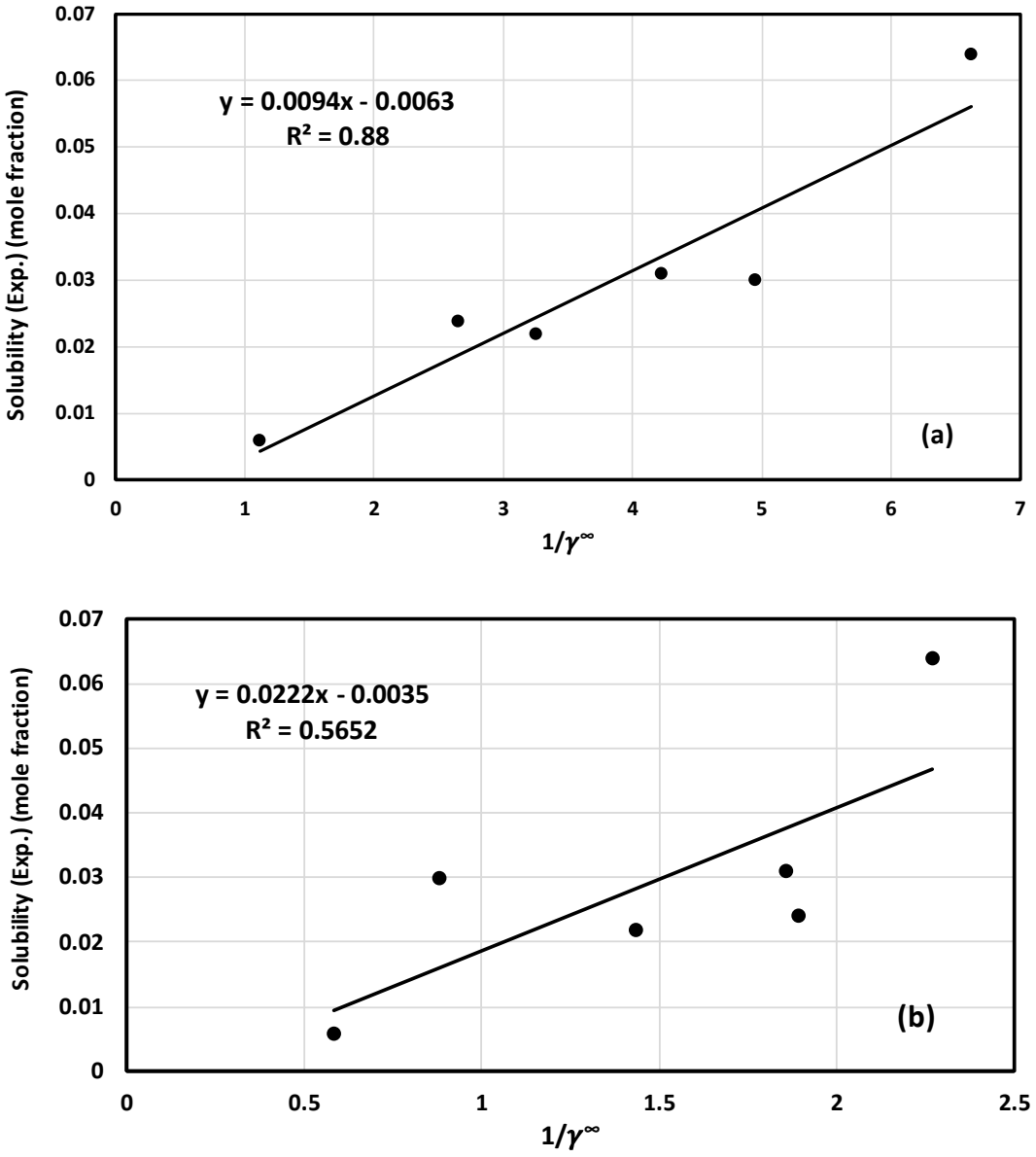

Figure 9: In fig. (a) and (b), the experimental solubility in mole fraction unit has been plotted as a function of $1/\gamma_{i/S}^{\infty}$ for the COSMOSAC-LANL and COSMOSAC-2013 model, respectively. These results have been shown for a particular metal complex $V(acac)_3$ in 6 different organic solvents.

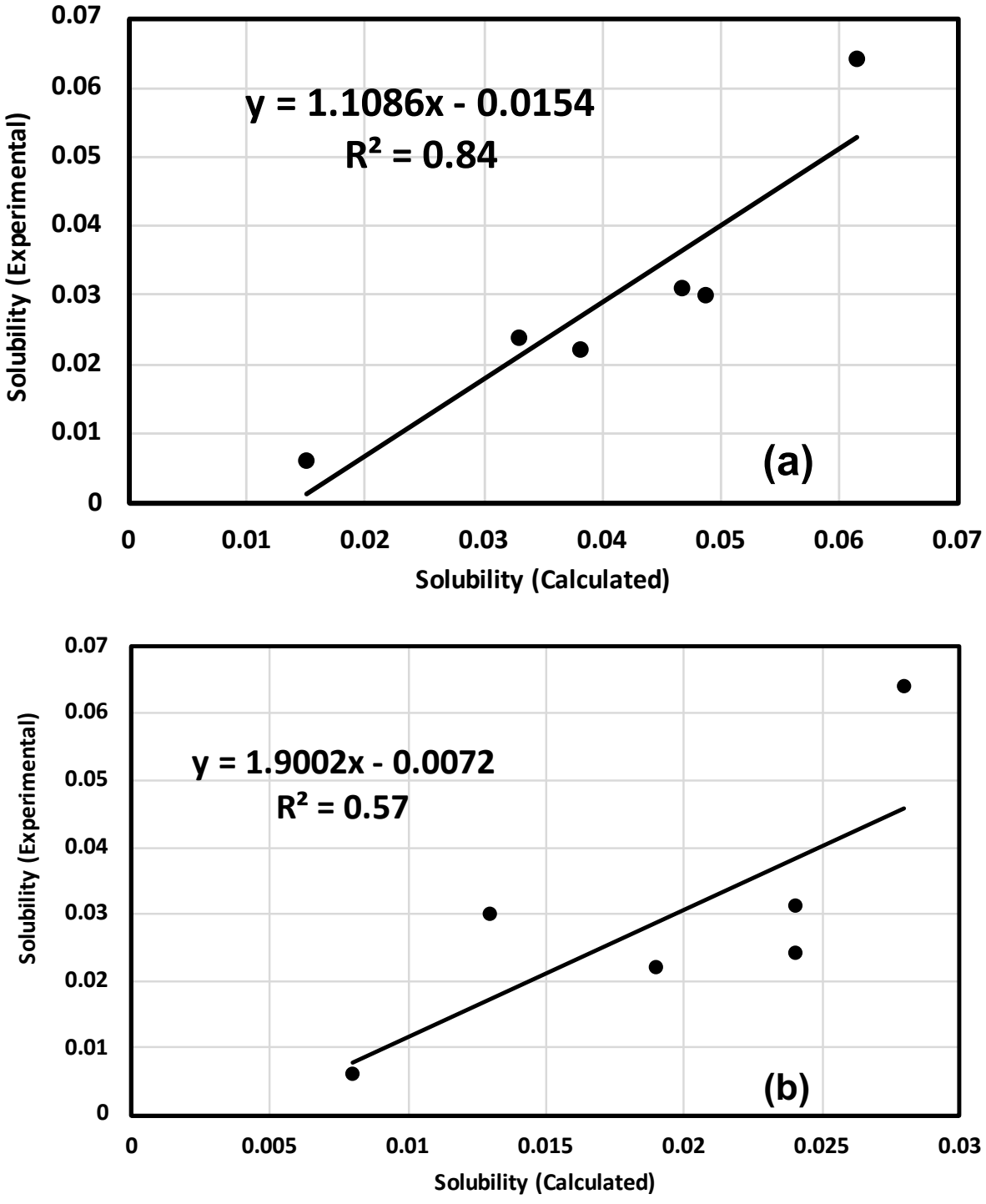

Figure 10: The experimental solubility vs calculated solubility for (a) COSMOSAC-LANL and (b) COSMOSAC-2013 model, respectively. The unit is in mole fraction.

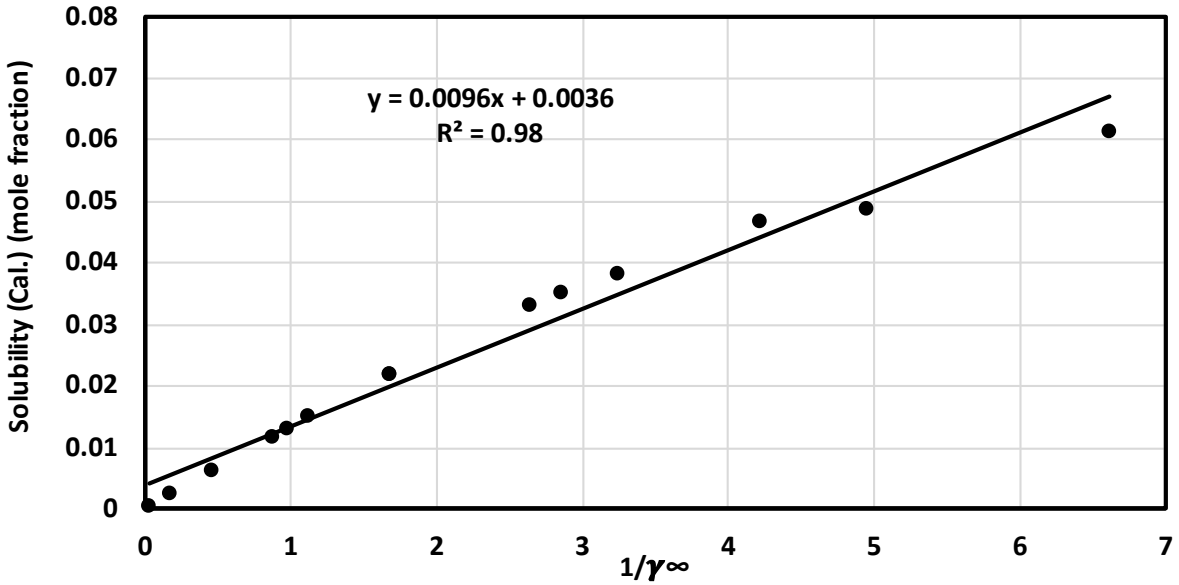

Figure 11: The calculated solubility in mole fraction unit has been plotted as a function of $1/\gamma_{i/S}^{\infty}$ using the COSMOSAC-LANL model for 14 different organic solvents.

the solubility trend observed incase of $V(acac)_3$ in six organic solvents. 1,3do dissolves maximum $V(acac)_3$ in its and thus shows maximum negative G^{ex} and ΔG^{mix}. To find the reason behind it, we calculated the Gibbs-Duhem relationship between these two species following the work reported in Ref. 32 and we noticed that for all cases the solubility of metal complex increases upon increasing the concentration of the organic solvent shown in Figure. 13 and therefore exhibit dual-solute effect.[32] The increase in the solubility causes decrease in the $\gamma_{i/S}^{\infty}$ according to Eq. 15. For the different organic solvents and a particular metal complex $V(acac)_3$, we noticed that the slopes in the respective curvatures vary a lot for the solvent showing maximum solubility of $V(acac)_3$ and the solvent is 1,3do in this case. This also indicates to the presence of the varying supramolecular interactions with the concentration and which is in good agreement with the previous results reported in the section 4 in this study for the acetonitrile solvent and in the work reported in Ref. 49. The dielectric constant of a solvent is one consequence of 3-dimensional hydrogen bonded type network present in a solvent. The dielectric constants for 1,3do, MA, ACN, DMPU, GBL and PC are 7.13 debye, 7.07 debye, 36.6 debye, 36.12 debye, 40.96 debye and 64 debye, respectively. It is known from electrochemistry that the ion association is promoted or enhanced with the decreasing dielectric constant of the solvent.[54] But, in these systems,

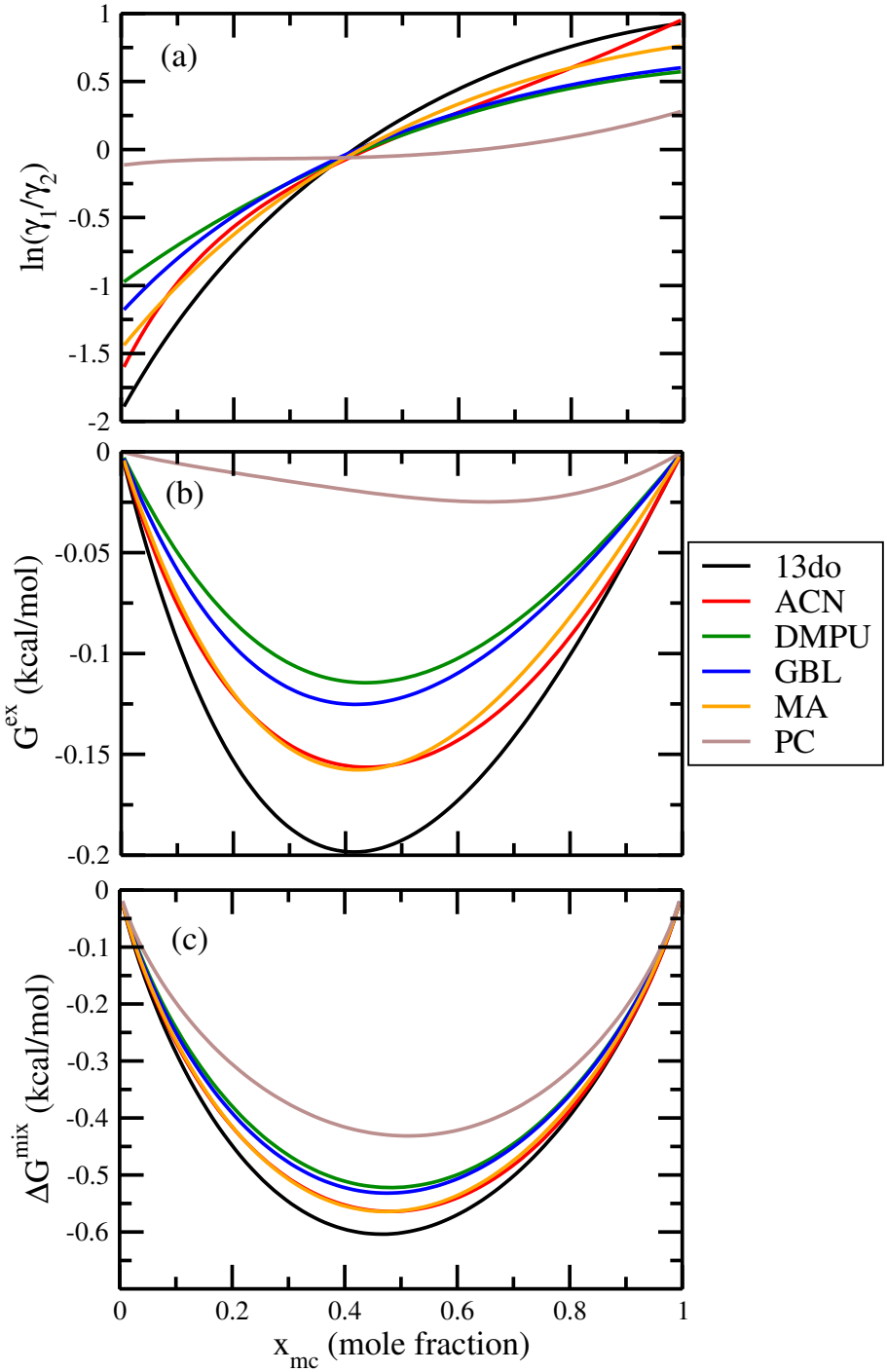

Figure 12: In fig(a) $\ln\gamma_1/\gamma_2$, in fig (b) G^{ex} and, in fig (c) ΔG^{mix} have been shown as a function of solute mole fraction for the $V(acac)_3$ metal complex in 6 different organic solvents. The γ_1 and γ_2 are the activity coefficient of the solute and solvent molecule, respectively.

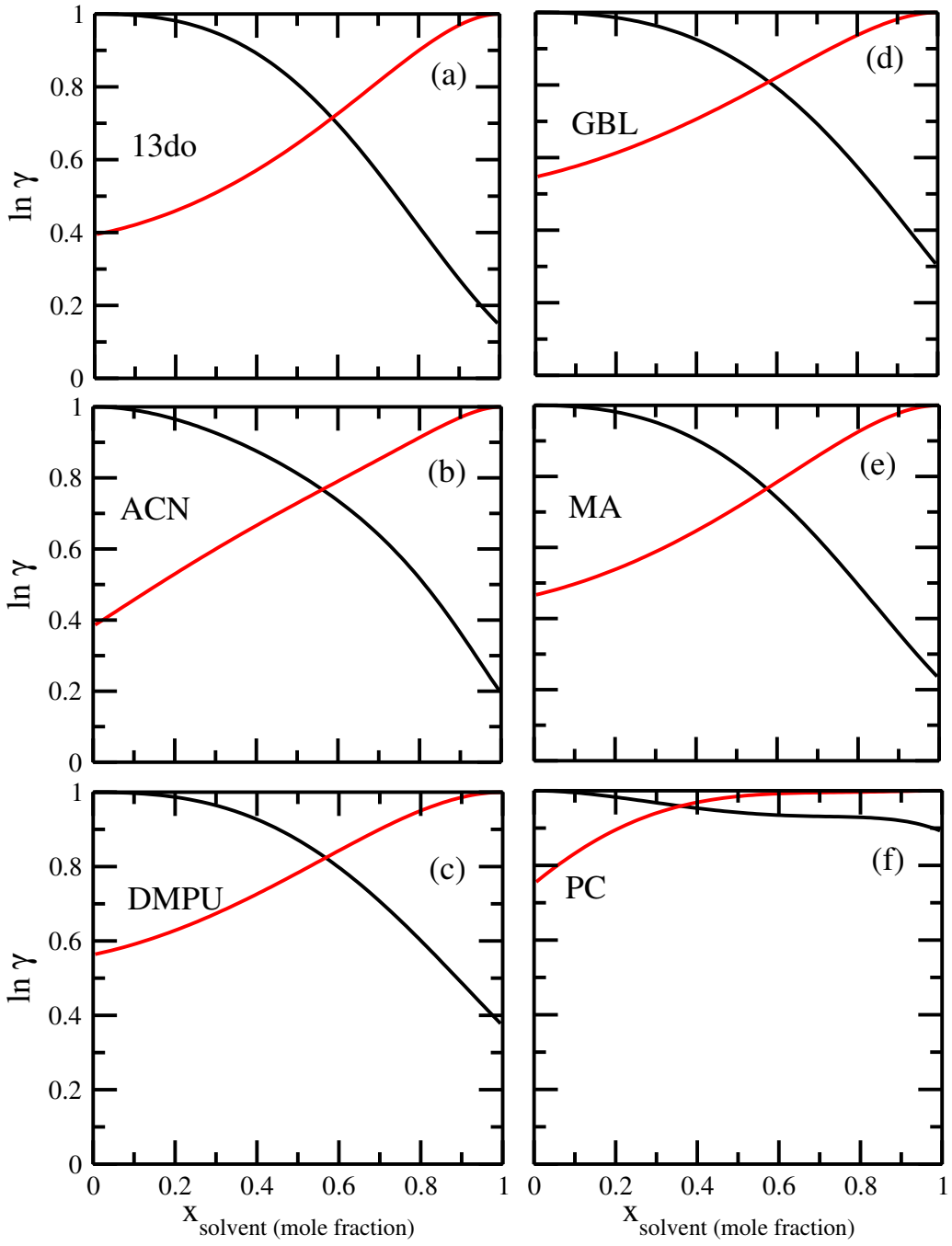

Figure 13: In all figures, lnγ has been plotted as a function of solvent mole fraction $x_{solvent}$ for 6 different organic solvents using the COSMOSAC-LANL model. The black curve is for the solute species and the red curve is for the solvent species.

there is no such distinct existence of the cation and anion because the all metal complexes are neutral.[11] Therefore, the solvent molecule will interact with the redox active species in place of the ion at the infinite dilute condition and thus, promotes the dissolution of the redox active species in it. From the present study, this fact is also strengthened for the non-aqueous redox flow cell. Except acetonitrile, we obtained a good correlation between the reported dielectric constant and p_σ(HB-Tot) for polar aprotic solvent with $R^2 = 0.91$. The result has been shown in Figure. S-11. The σ profile for the 6 organic solvents have been given in Figure. 14. σ profile is a unique feature of a compound i.e., no two compounds will have the similar σ profile. The σ profile of all 14 organic solvents have been given in Figure. S-12 in the supporting information and the Gibbs-Duhem relationship for 13 different metal complexes in acetonitrile solvent has been shown in Figure. S-7 and S-8 in the supporting information. We found that the dual-solute effect prevails for all metal complexes in acetonitrile solvent. Similar results have been observed in case of metal complex solubility in ionic liquids.[32] The dual solute effect can either promote the solubility or impede it. A conclusion can be made from these observations that the dual-solute effect is a characteristic feature of the interaction between the solute and non-aqueous solvent molecule in the non-aqueous redox flow cell.

We observed a strong correlation between the σ profile due to the hydrogen bond type of interaction in solvent molecule and the experimental solubility of metal complex in section 5. The solvent molecule with least amount of p_σ(HB-Tot) profile dissolves more redox active species. The calculated p_σ(HB-Tot) for 14 organic solvent has been given in Table. 5. We correlate the solubility of $V(acac)_3$ in six organic solvents with the p_σ(HB-Tot) of the solvents and obtained a correlation of $R^2 = 0.70$. The result is shown in Figure. 15. This inverse correlation between the experimental solubility and p_σ(HB-Tot) indicates when the solubility of an active species will cost high Gibbs free energy of cavity formation, it will be less dissolved in the organic solvent. Therefore, the solubility of the active species will decrease. We use those informations to screen the 14 different metal complexes and the 6 different organic solvents against each other to find the best pair of metal complex and organic solvent to increase the energy density of a particular non-aqueous redox flow cell. The linear correlation between the experimental solubility

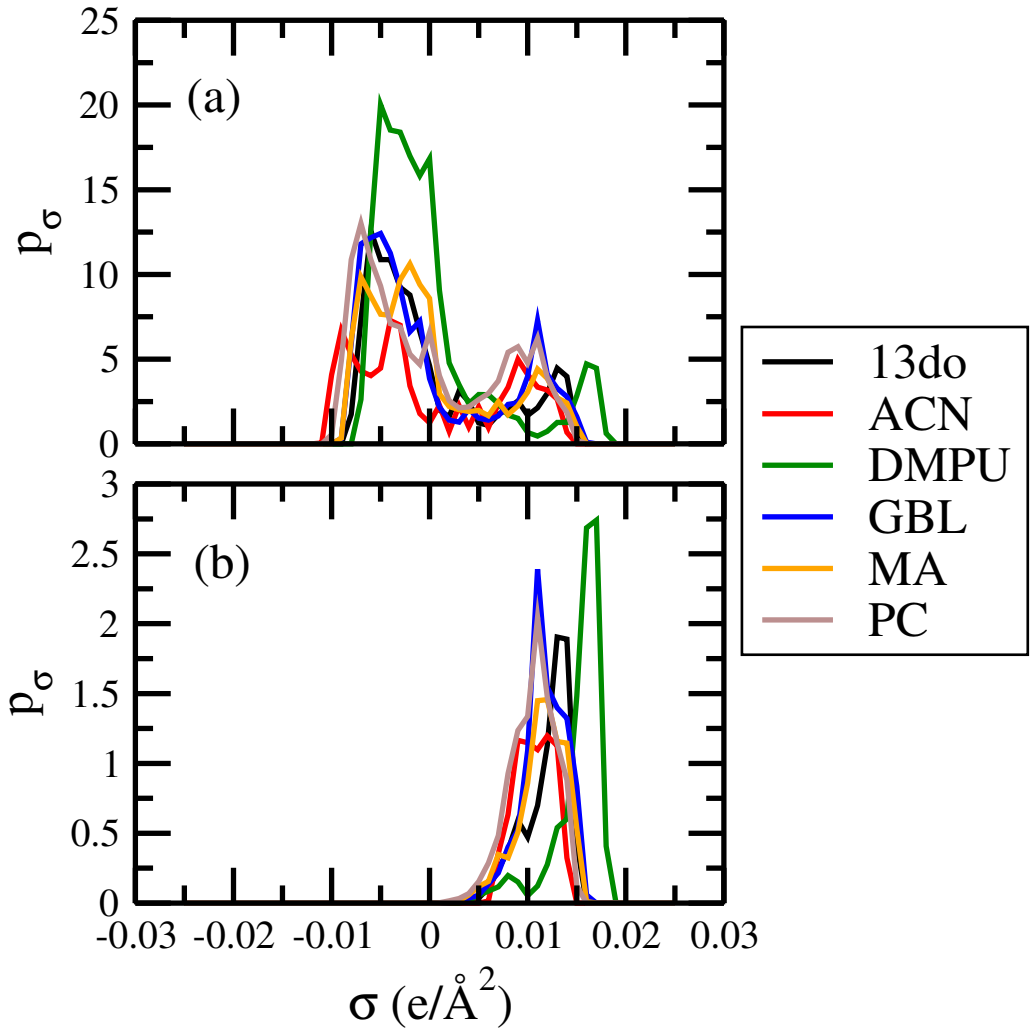

Figure 14: In fig (a), the total σ profile has been shown for 6 organic solvents. In fig (b), the p_σ(HB-Tot) has been shown for 6 organic solvents.

and the p_σ(HB-Tot) is 85% for 14 different transition metal complexes for a particular organic solvent acetonitrile. This result has been shown in Figure. S-9(b). However, this can be improved by using the COSMOSAC-LANL model with optimized parameters for the metal complexes and organic solvents. We defined a new solubility parameter (χ) for a binary mixture, where $\chi = \frac{p_\sigma^{\mathrm{mc}}(HB-Tot)}{p_\sigma^{\mathrm{solvent}}(HB-Tot)}$. The results for 14×6 binary mixtures are shown in Figure. 15. The accuracy of this 14×6 (84) screening model should vary within 70% - 85%. We also noticed that among this 14×6 screening model 14×5 (70) system will be screened within the accuracy range between 84% - 85%. The accuracy of 10×6 (60) was within 70% - 80%. A much better 9×4 (36) and 8×4 (32) system can be screened within the accuracy range 90% - 99.7% and 96% - 99.7%, respectively using the model. The list of metal complexes and organic solvents for 14×5 (70), 10×6 (60), 9×4 (36) and 8×4 (32) screening have been given in Table. 2 and 5. From the calculations, we reached to this conclusion that along the X-axis of the screening plot, the metal complexes will be screened against a particular organic solvent with accuracy stated for the metal complex screening against the organic solvent acetonitrile (Figure. S-9(b)) and along the Y-axis, the solvent will be screened against a particular metal complex with accuracy obtained for the solvent screening against the V(acac)$_3$ metal complex (Figure. 15 (top)) because these two informations have been used to propose the solubility parameter χ. The all necessary plots for 14×6 (84), 14×5 (70), 10×6 (60), 9×4 (36) and 8×4 (32) screen have been given in Figures. (S-13) - (S-17), respectively in the supporting information. To validate our calculations, we chose polar protic, polar aprotic and non-polar solvents. The polar aprotic solvent appears as most suitable solvent for non-aqueous redox flow cell according to the present study. Therefore, we conclude that the compatible pair of redox active species and organic solvent should have the stability due to the hydrogen-bonded type of attractive interaction in the binary mixture. We have chosen this method because ability to interact through the hydrogen-bonded type of interaction in the redox active species should increase the solubility of active species in the organic solvent according to Figure. 8 while the more hydrogen-bonded type of interaction in the organic solvent will decrease the solubility of the active species shown in Figure. 15. This observation in the results also strengthens the fact that the solubility of the active species will always has direct

relationship with its p_σ(HB-Tot) and inverse relationship with the solvent p_σ(HB-Tot). These can be seen in Figure. 8 and 15. The above fact has been strengthened by the results obtained from our previous study on CO_2 solubility in ionic liquids[38] and metal complex solubility in ionic liquids.[32] It has been observed that the solubility of both the CO_2 and metal complex increases in ionic liquid with the decreasing percentage of the σ profile due to the hydrogen-bonded type of interaction. The results have been shown for 31 ionic liquids for CO_2 solubility in ionic liquids and for 9 ionic liquids for metal complex solubility in ionic liquids. This is indicative to the important role by the hydrogen-bonded type of interaction in the solubility of a particular solute in ionic liquid. The results have been shown in Figure. 16. It is to be noted that for a particular solute molecule we correlated the experimental solubility of the solute species with the $\%p_\sigma$(HB-Tot) of the ionic liquids while for a particular solvent and for the organic solvents we correlated the experimental solubility with the p_σ(HB-Tot). This knowledge motivates us to define the solubility parameter χ for the metal complexes solubility in organic solvents. At last, we propose a regression model to screen the metal complexes for a particular organic solvent and organic solvents for a particular metal complex in Figure. S-18-19 in the supporting information, respectively in terms of χ.

Organic Solvents	p_σ(HB-Tot)(Å^2)	p_σ(Total)(Å^2)	$\%p_\sigma$(HB-Tot)
Cyclohexane	0.0	138.491	0.0
DIPE	4.13	165.040	2.502
1-Butanol	9.19	130.662	7.033
1-Hexanol	9.17	171.489	5.347
1-Hexyne	0.0	151.286	0.0
1-Heptyne	0.0	172.052	0.0
1-Hexene	0.0	154.443	0.0
Benzene	0.0	123.095	0.0
1,3do	7.88	106.589	7.392
ACN	7.06	83.684	8.436
DMPU	9.54	169.906	5.615
GBL	10.03	120.124	8.349
MA	8.14	115.233	7.064
PC	10.21	131.041	7.792

Table 5: The p_σ(HB-Tot), p_σ(Total) and $\%p_\sigma$(HB-Tot) of 14 different organic solvents.

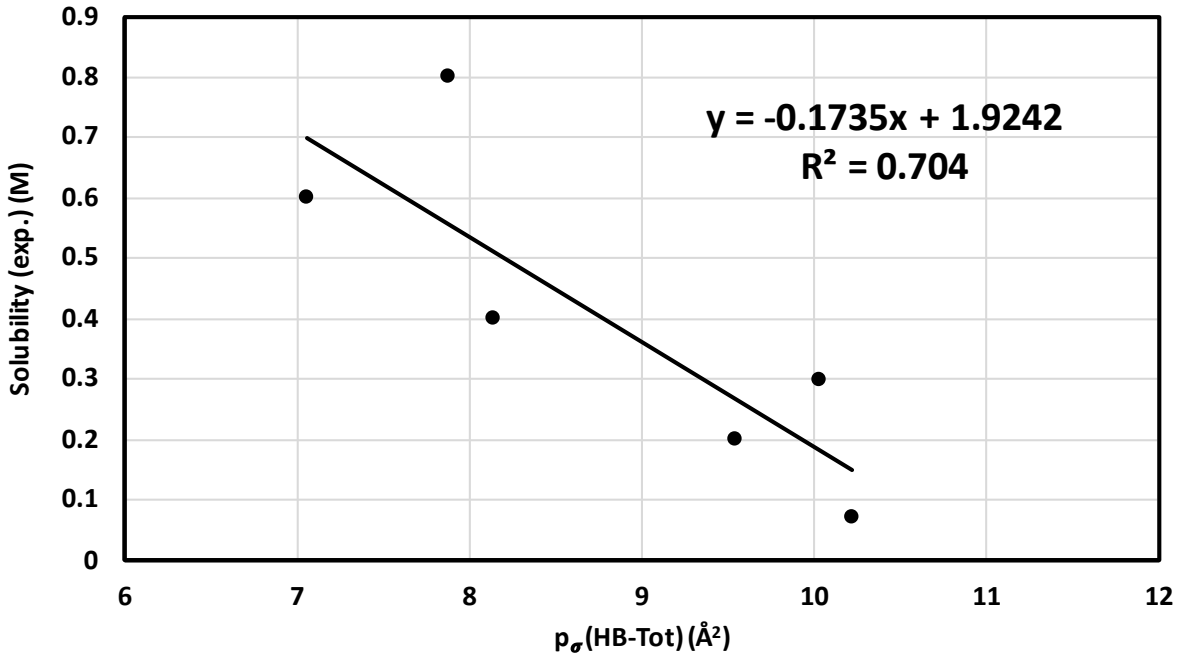

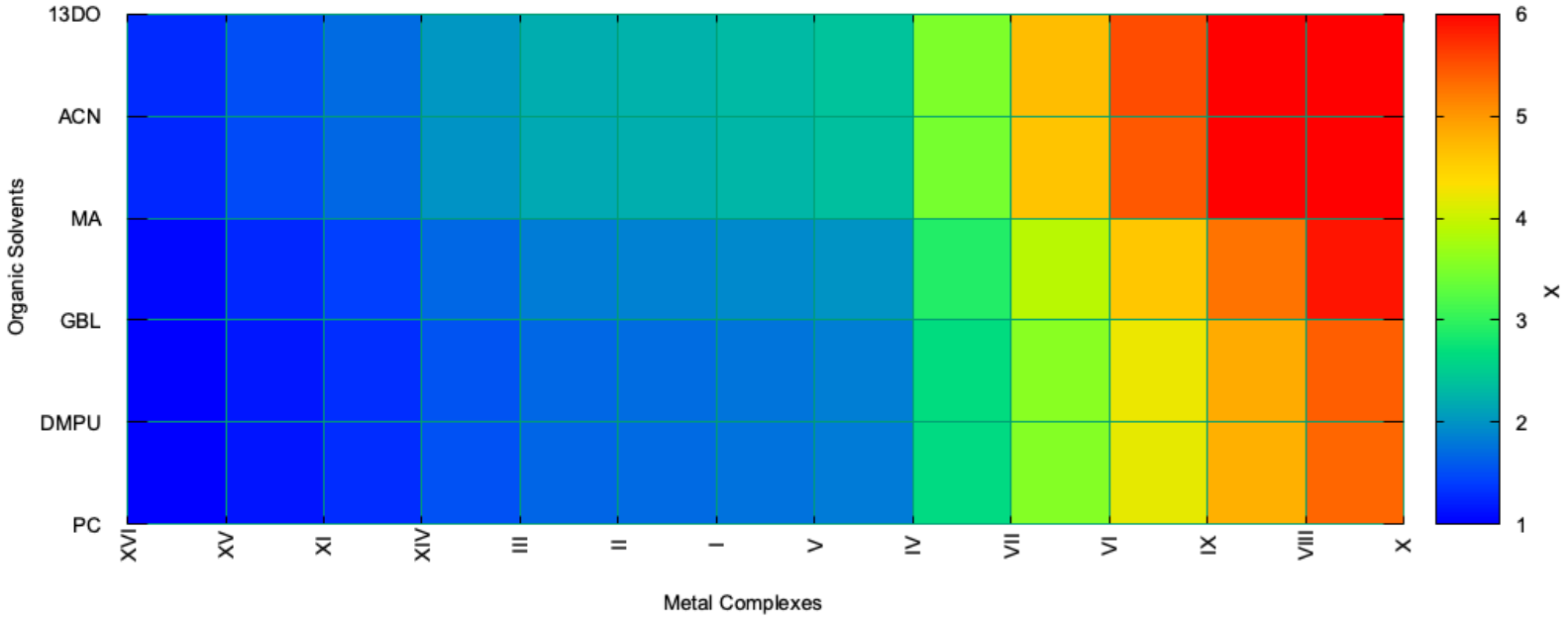

Figure 15: (top) The experimental solubility of $V(acac)_3$ in 6 different organic solvents have been correlated with the p_σ(HB-Tot) for 6 organic solvents. (bottom) Screening of 14 different transition metal complexes and 6 different organic solvents to determine the best pair of redox active species and organic solvent to increase the energy density of non-aqueous redox flow cell based on the solubility parameter (χ) information. More χ means more solubility in the colorbar (righthand side).

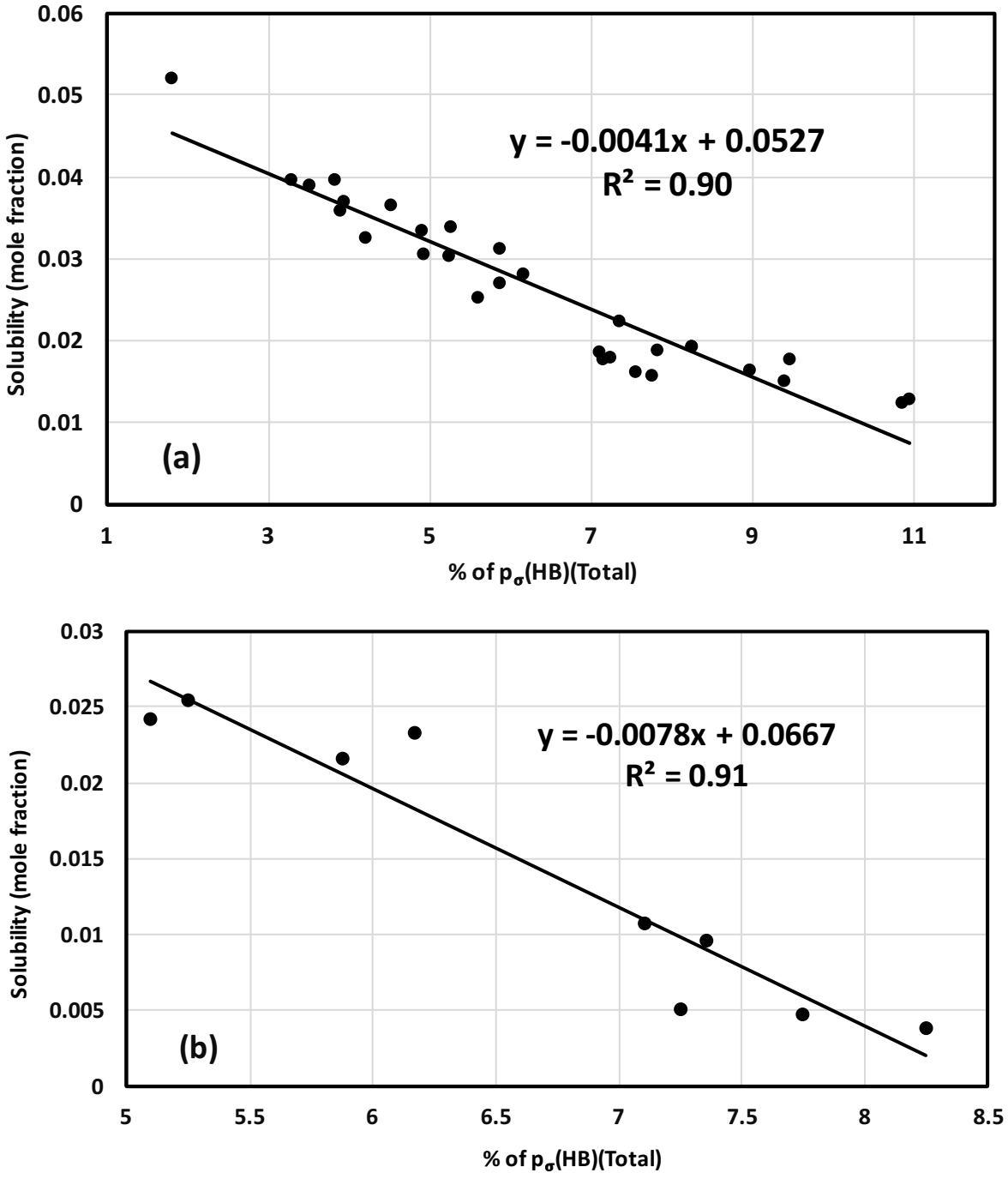

Figure 16: (a) CO_2 solubility in ionic liquids vs $\%p_\sigma$(HB)(Total). (b) Metal complex solubility in ionic liquids vs $\%p_\sigma$(HB)(Total). The ionic liquids have been taken from the Refs. 32 and 38. In (a), all solubility results reported here is experimental solubility taken from the references given in Ref. 38. In (b), the all solubilities are directly taken from Ref. 32.

7 Conclusion

A series of *ab initio* calculations have been performed to propose a solubility model for 16 different transition metal complexes in acetonitrile organic solvent. Using our calculations, we have shown how one will be able to effectively screen the transition metal complexes for a particular organic solvent and organic solvents for a particular metal complexes to increase the energy density of the non-aqueous redox flow cell. We use the COSMOSAC-LANL model to explain the solvation mechanism of the transition metal complexes in certain organic solvents. We applied the model over 14 different organic solvents for a particular transition metal complex $V(acac)_3$. The solubility of $V(acac)_3$ in 6 organic solvents has been calculated using the COSMOSAC-LANL model and compared with the experimental results where they are available. To explain the solvation mechanism, we calculated G^{ex} *vs* x_{mc}, ΔG^{mix} *vs* x_{mc} and $\ln\left(\frac{\gamma_{i/S}^{\text{LANL}}}{\gamma_{j/S}^{\text{LANL}}}\right)$ *vs* x_{mc}. The organic solvent showing maximum solubility of $V(acac)_3$ in it has lowest $\gamma_{i/S}^{\infty}$. Dual solute effect and Gibbs-Duhem relationship in a binary mixture have been verified by computing $\ln\gamma$ *vs* x_{solvent} and $\ln\gamma$ *vs* x_{mc}. The solubility of the transition metal complexes has been correlated with the χ $(\frac{p_{\sigma}^{\text{mc}}(HB-Total)}{p_{\sigma}^{\text{solvent}}(HB-Total)})$. First time, we were able to address the issue related to the hydrogen-bonded type interaction between the solute and solvent molecules and how the interaction promote or obstruct the solubility, using the first principle COSMO based continuum solvation model. According to our study this interaction in a binary mixture is responsible for the stability of the solution also. We noticed from our study that enhanced hydrogen-bonded type interaction between these two species is the main cause of their solubility in a non-aqueous media. Using the model, we were also quantify those interactions present between them. The new model was able to explain the solubility of a transition metal complexes and find the exact reason behind the experimental solubility of them and has been used to screen the 14 different organic solvents for a particular metal complex $V(acac)_3$ with R^2=0.98. We also proposed a simple method to determine the solubility of transition metal complexes with different ligands but same metal center with R^2=0.82 and transition metal complexes with same ligands but different metal center with R^2=0.82. For the transition metal complexes with different ligands but same metal center

we observed that the χ of individual metal complex correlates with the experimental solubility with 90% precision for 10 different transition metal complexes for which the reported experimental solubility is good. For the transition metal complex with similar ligand but different metal center, we correlate ($R^2 = 0.98$) the solubility with the $1/\gamma^{\infty}_{i/S}$, when the experimental solubility was not reported. When the correlation between the experimental solubility and χ has been made for all 16 metal complexes, the observed correlation was 75% which upon removal of the two outliers (XII and XIII) increases to 85% precision. We observed that the coefficient of determination ($R^2 = 0.75$) is very closer to the R^2 value reported in the work stated in Ref. 14. It is noteworthy in this regard that the solubility parameters in that work were optimized, while that was not the case for our model. Therefore, we believe that our model will improve more, (i) when we will have more experimental data in our hand, that will help improving the statistics of the model and (ii) when the optimized parameters will present in the models for the species of interest in this case. The model can also be improved by using other high level quantum calculations. But, since this model is a linear regression model, therefore parameter optimization is required. In the present study our main motivation was to find the underlying principle behind the solubility of transition metal complexes in non-aqueous redox flow cell and in all cases, we noticed that the coefficient of determination (R^2) was greater than or equal to 70% in few cases and it was between 80% - 100% in most of the cases. These coefficient of determinations were within the range of reported coefficient of determination (which is 0.79) in Ref. 14. We also noticed that the accuracy of the calculated solubility using the COSMOSAC-LANL model outperforms the results obtained using the COSMOSAC-2013 model. This is happened due to the modified combinatorial term present in the model. The combinatorial term had been modified by a factor of 2 as a consequence of first principle calculation. We observed a good correlation between the calculated and the experimental solubility data of $V(acac)_3$ in organic solvents where they were available. The corresponding results have been shown in Figures. 9 - 10.

We used all these information to screen 14 different transition metal complexes and 6 different organic solvents (i.e., total $14\times6 = 84$ binary mixtures) to predict the best compatible pair of redox active species and organic solvent to increase the energy density

of the non-aqueous redox flow cell. The current study was able to capture the variation of the supramolecular forces with the species concentration in the solvent. A complicated variation has been noticed in this case. According to the study, a particular stoichiometry corresponding to a particular complex structure dominates the stable solution. The new model is able to predict the suitable solvent and the redox active species to construct an efficient non-aqueous redox flow cell with increasing energy density. Based on our calculations, the polar aprotic solvent such as 1,3do and acn appear as suitable solvent and the ester substituted tris-acetyleacetonate transition metal complexes such as VI, VII, VIII, IX and X appear as suitable redox active species. The theoretical results reported in this study are found to be in good agreement with the experimental and theoretical results already reported elsewhere.[4,14,46] The solubility results presented in this study have been first time explained from the microscopic point of view and using the basic principles of solvation and solution chemistry and COSMOSAC-LANL theory. The information based on the σ profile will be used to design future redox active species and the organic solvent for better energy density in non-aqueous redox flow cell. The physical insight to the solubility can be obtained using the new model. The model can be used to screen the redox active species and the non-aqueous solvents against each other and will be further improved based on the research requirement in future.

8 Acknowledgement

The research leading to these results was funded by the "Laboratory Directed Research and Development" program grant no. 20170046DR in Los Alamos National Laboratory, USA. Los Alamos National Laboratory is operated by Triad National Security under contract number 89233218CNA000001 for the Department of Energy.

9 Conflicts of Interest

There are no conflicts of interest to declare

Appendix A

The Staverman-Guggenheim (SG)[39,40,55] combinatorial term is based on the Flory-Huggins model, however the SG term also consider the interaction between the solute ($i = 1$) and solvent ($j = 2$) species due their shape differences to some extent. The combinatorial term proposed in the UNIQUAC model was

$$\frac{g^E(COMB)}{RT} = x_1 \ln\frac{\phi_1}{x_1} + x_2 \ln\frac{\phi_2}{x_2} + \frac{z}{2}\left(q_1 x_1 \ln\frac{\phi_1}{x_1} + q_2 x_2 \ln\frac{\phi_2}{x_2}\right) \tag{13}$$

for the binary mixture system using the local composition theory. z is the coordination number equal to 10. The fraction volume ($\phi_{\rm i}$) and surface area ($\theta_{\rm i}$) are as

$$\phi_{\rm i} = \frac{x_{\rm i} r_{\rm i}}{\sum_{j=1}^{2} x_{\rm j} r_{\rm j}} \text{ and } \theta_{\rm i} = \frac{x_{\rm i} q_{\rm i}}{\sum_{j=1}^{2} x_{\rm j} q_{\rm j}} \text{ , respectively ,} \tag{14}$$

where, $r_{\rm i}$ and $q_{\rm i}$ are the normalized volume and surface area of species i=1,2.

The activity coefficient will be obtained from the above expression[43]

$$\left(\frac{\partial n G^{\rm ex}}{\partial n_{\rm i}}\right)_{T,P,n_{\rm i\neq j}} = RT\ln(\gamma_{\rm i}) \tag{15}$$

for the species i=1,2. The Staverman-Guggenheim (SG) combinatorial for solute and solvent species is

$$\ln(\gamma_{\rm i/S}^{\rm comb}) = 1 - \frac{\phi_{\rm i}}{x_{\rm i}} + \ln\frac{\phi_{\rm i}}{x_{\rm i}} - \frac{z}{2} q_{\rm i}\left(1 - \frac{\phi_{\rm i}}{\theta_{\rm i}} + \ln\frac{\phi_{\rm i}}{\theta_{\rm i}}\right). \tag{16}$$

For solute species(1), one can write the above equation as

$$\ln(\gamma_{\rm 1/S}^{\rm comb}) = 1 - \frac{\phi_1}{x_1} + \ln\frac{\phi_1}{x_1} - \frac{z}{2} q_1\left(1 - \frac{\phi_1}{\theta_1} + \ln\frac{\phi_1}{\theta_1}\right) \tag{17}$$

where, the fraction volume (ϕ_1) and surface area (θ_1) are as

$$\phi_1 = \frac{x_1 r_1}{x_1 r_1 + x_2 r_2} \text{ and } \theta_1 = \frac{x_1 q_1}{x_1 q_1 + x_2 q_2} \text{ , respectively ,} \tag{18}$$

where, r_1 and q_1 are the normalized volume and surface area of solute, respectively, while r_2 and q_2 are the normalized volume and surface area for solvent species, respectively. x_1 and x_2 are the mole fractions of solute and solvent species, respectively. Now suppose r_1' and q_1' are the unnormalized volume and surface area for solute species obtained from

COSMO calculations, then one can write $r_1 = \frac{r'_1}{r_0}$ and $q_1 = \frac{q'_1}{q_0}$, where r_0 and q_0 are 66.69 Å^3 and 79.53 Å^2, respectively. Now, if one substitute r_1 and q_1 in Eq. 18, one will get

$$\phi_1 = \frac{x_1 r'_1/r_0}{x_1 r'_1/r_0 + x_2 r'_2/r_0} \text{ and } \theta_1 = \frac{x_1 q'_1/q_0}{x_1 q'_1/q_0 + x_2 q'_2/q_0} \text{ , respectively .} \tag{19}$$

Therefore,

$$\phi_1 = \frac{x_1 r'_1}{x_1 r'_1 + x_2 r'_2} \text{ and } \theta_1 = \frac{x_1 q'_1}{x_1 q'_1 + x_2 q'_2} \text{ , respectively .} \tag{20}$$

Now if one substitutes ϕ_1, θ_1 and q_1 in the Eq. 17, one will obtain

$$\ln(\gamma^{\text{comb}}_{1/\text{S}}) = 1 - \left(\frac{\frac{x_1 r'_1}{x_1 r'_1 + x_2 r'_2}}{x_1}\right) + \ln\left(\frac{\frac{x_1 r'_1}{x_1 r'_1 + x_2 r'_2}}{x_1}\right) - \frac{z}{2}\frac{q'_1}{q_0}\left[1 - \left(\frac{\frac{x_1 r'_1}{x_1 r'_1 + x_2 r'_2}}{\frac{x_1 q'_1}{x_1 q'_1 + x_2 q'_2}}\right) + \ln\left(\frac{\frac{x_1 r'_1}{x_1 r'_1 + x_2 r'_2}}{\frac{x_1 q'_1}{x_1 q'_1 + x_2 q'_2}}\right)\right]. \tag{21}$$

By simplifying, the above equation can be written as

$$\ln(\gamma^{\text{comb}}_{1/\text{S}}) = 1 - \left(\frac{r'_1}{x_1 r'_1 + x_2 r'_2}\right) + \ln\left(\frac{r'_1}{x_1 r'_1 + x_2 r'_2}\right) - \frac{z}{2}\frac{q'_1}{q_0}\left[1 - \left(\frac{\frac{r'_1}{x_1 r'_1 + x_2 r'_2}}{\frac{q'_1}{x_1 q'_1 + x_2 q'_2}}\right) + \ln\left(\frac{\frac{r'_1}{x_1 r'_1 + x_2 r'_2}}{\frac{q'_1}{x_1 q'_1 + x_2 q'_2}}\right)\right]. \tag{22}$$

$$\ln(\gamma^{\text{comb}}_{1/\text{S}}) = 1 - \left(\frac{r'_1}{x_1 r'_1 + x_2 r'_2}\right) + \ln\left(\frac{r'_1}{x_1 r'_1 + x_2 r'_2}\right) - \frac{z}{2} q_1\left[1 - \left(\frac{\frac{r'_1}{x_1 r'_1 + x_2 r'_2}}{\frac{q'_1}{x_1 q'_1 + x_2 q'_2}}\right) + \ln\left(\frac{\frac{r'_1}{x_1 r'_1 + x_2 r'_2}}{\frac{q'_1}{x_1 q'_1 + x_2 q'_2}}\right)\right]. \tag{23}$$

Similarly, one can write this expression for solvent species,

$$\ln(\gamma^{\text{comb}}_{2/\text{S}}) = 1 - \left(\frac{r'_2}{x_1 r'_1 + x_2 r'_2}\right) + \ln\left(\frac{r'_2}{x_1 r'_1 + x_2 r'_2}\right) - \frac{z}{2}\frac{q'_2}{q_0}\left[1 - \left(\frac{\frac{r'_2}{x_1 r'_1 + x_2 r'_2}}{\frac{q'_2}{x_1 q'_1 + x_2 q'_2}}\right) + \ln\left(\frac{\frac{r'_2}{x_1 r'_1 + x_2 r'_2}}{\frac{q'_2}{x_1 q'_1 + x_2 q'_2}}\right)\right]. \tag{24}$$

$$\ln(\gamma^{\text{comb}}_{2/\text{S}}) = 1 - \left(\frac{r'_2}{x_1 r'_1 + x_2 r'_2}\right) + \ln\left(\frac{r'_2}{x_1 r'_1 + x_2 r'_2}\right) - \frac{z}{2} q_2\left[1 - \left(\frac{\frac{r'_2}{x_1 r'_1 + x_2 r'_2}}{\frac{q'_2}{x_1 q'_1 + x_2 q'_2}}\right) + \ln\left(\frac{\frac{r'_2}{x_1 r'_1 + x_2 r'_2}}{\frac{q'_2}{x_1 q'_1 + x_2 q'_2}}\right)\right]. \tag{25}$$

The above two expressions stated in Eqs. 24 and 25 have been used in the expression of SG term used in COSMOSAC-LANL model.

Appendix B

The excess free energy of a binary solution can be written using 3-suffix Margules function[41,42]

$$G^{\text{ex}} = x_1 x_2 (A_{21} x_1 + A_{12} x_2) \tag{26}$$

where, x_1 and x_2 are the mole fractions for solute ($i = 1$) and solvent ($j = 2$) molecules in a binary mixture and A_{21} and A_{12} are the Margules parameters. The expression for total excess free energy for n total mole number of species is

$$nG^{\text{ex}} = \frac{n_1 n_2}{(n_1 + n_2)^2} (A_{21} n_1 + A_{12} n_2)\,. \tag{27}$$

n_1 and n_2 are the number of moles of solute and solvent, respectively. Differentiating the above equation with respect to n_1, one will get,

$$\left(\frac{\partial n G^{\text{ex}}}{\partial n_1} \right)_{T,P,n_2} = RT \ln(\gamma_1) \tag{28}$$

$$\rightarrow RT \ln \gamma_1 = n_{\text{j}} \left[(A_{21} n_1 + A_{12} n_2) \left(\frac{1}{(n_1 + n_2)^2} - \frac{2n_1}{(n_1 + n_2)^3} \right) + \frac{n_1 A_{21}}{(n_1 + n_2)^2} \right] \tag{29}$$

$$\rightarrow RT \ln \gamma_1 = \frac{n_2}{(n_1 + n_2)} \left[\frac{(A_{21} n_1 + A_{12} n_2)}{(n_1 + n_2)} \left(1 - \frac{2n_1}{(n_1 + n_2)} \right) + \frac{n_1 A_{21}}{(n_1 + n_2)} \right] \tag{30}$$

Reconversion of n_{i} to x_{i} will give

$$RT \ln \gamma_1 = x_2 \left[(A_{21} x_1 + A_{12} x_2)(1 - 2x_1) + A_{21} x_1 \right] \tag{31}$$

$$RT \ln \gamma_1 = x_2 \left[(A_{21} x_1 + A_{12} x_2) - 2x_1 (A_{21} x_1 + A_{12} x_2) + A_{21} x_1 \right] \tag{32}$$

$$RT \ln \gamma_1 = x_2 \left[2A_{21} x_1 + A_{12} x_2 - 2A_{21} x_1^2 - 2A_{12} x_1 x_2 \right] \tag{33}$$

As we know that : $x_1 = 1 - x_2$, therefore, we can write the above equation as

$$RT \ln \gamma_1 = x_2 \left[2A_{21} x_1 + A_{12} x_2 - 2A_{21} x_1 (1 - x_2) - 2A_{12} x_1 x_2 \right] \tag{34}$$

$$RT \ln \gamma_1 = x_2^2 \left[A_{12} + 2 \left(A_{21} - A_{12} \right) x_1 \right] \tag{35}$$

Subsituting $x_1 = 1 - x_2$ in the above equation, one will get

$$\rightarrow A_{12}x_2^2 + 2(A_{21} - A_{12})(x_2^2 - x_2^3) \tag{36}$$

$$\rightarrow A_{12}x_2^2 + \left(2A_{21}x_2^2 - 2A_{21}x_2^3 - 2A_{12}x_2^2 + 2A_{12}x_2^3\right) \tag{37}$$

Further simplifying the above equation one will get

$$RT\ln\gamma_1 = \left(2A_{21} - A_{12}\right)x_2^2 + \left(2A_{12} - 2A_{21}\right)x_2^3 \tag{38}$$

Now equating $\alpha_1 = \left(2A_{21} - A_{12}\right)$ and $\beta_1 = \left(2A_{12} - 2A_{21}\right)$, one can write Eq. 38 as

$$\ln\gamma_1 = \frac{\alpha_1 x_2^2 + \beta_1 x_2^3}{RT} \tag{39}$$

Similarly, for species 2, differentiating the above Eq. 26 with respect to n_2, one will get,

$$\left(\frac{\partial nG^{\text{ex}}}{\partial n_2}\right)_{T,P,n_1} = RT\ln(\gamma_2) \tag{40}$$

$$\rightarrow RT\ln\gamma_2 = n_1\left[(A_{21}n_1 + A_{12}n_2)\left(\frac{1}{(n_1+n_2)^2} - \frac{2n_2}{(n_1+n_2)^3}\right) + \frac{n_2A_{12}}{(n_1+n_2)^2}\right] \tag{41}$$

$$\rightarrow RT\ln\gamma_2 = \frac{n_1}{(n_1+n_2)}\left[\frac{(A_{21}n_1 + A_{12}n_2)}{(n_1+n_2)}\left(1 - \frac{2n_2}{(n_1+n_2)}\right) + \frac{n_2A_{12}}{(n_1+n_2)}\right] \tag{42}$$

Reconversion of n_{i} to x_{i} will give

$$RT\ln\gamma_2 = x_1\left[(A_{21}x_1 + A_{12}x_2)(1 - 2x_2) + A_{12}x_2\right] \tag{43}$$

$$RT\ln\gamma_2 = x_1\left[(A_{21}x_1 + A_{12}x_2) - 2x_2(A_{21}x_1 + A_{12}x_2) + A_{12}x_2\right] \tag{44}$$

$$RT\ln\gamma_2 = x_1\left[2A_{12}x_2 + A_{21}x_1 - 2A_{12}x_2^2 - 2A_{21}x_1x_2\right] \tag{45}$$

As we know that : $x_2 = 1 - x_1$, therefore, we can write the above equation as

$$RT\ln\gamma_2 = x_1\left[2A_{12}x_2 + A_{21}x_1 - 2A_{12}x_2(1 - x_1) - 2A_{21}x_1x_2\right] \tag{46}$$

$$RT\ln\gamma_2 = x_1^2\left[A_{21} + 2\left(A_{12} - A_{21}\right)x_2\right] \tag{47}$$

Substituting $x_2 = 1 - x_1$ in the above equation, one will get

$$\rightarrow A_{21}x_1^2 + 2(A_{12} - A_{21})(x_1^2 - x_1^3) \tag{48}$$

$$\rightarrow A_{21}x_2^2 + \left(2A_{12}x_1^2 - 2A_{12}x_1^3 - 2A_{21}x_1^2 + 2A_{21}x_1^3\right) \tag{49}$$

Further simplifying of the above equation one will get

$$RT\ln\gamma_2 = \left(2A_{12} - A_{21}\right)x_1^2 + \left(2A_{21} - 2A_{12}\right)x_1^3 \tag{50}$$

Now equating $\alpha_2 = \left(2A_{12} - A_{21}\right)$ and $\beta_2 = \left(2A_{21} - 2A_{12}\right)$, one can write Eq. 50 as

$$\ln\gamma_2 = \frac{\alpha_2 x_1^2 + \beta_2 x_1^3}{RT}\,. \tag{51}$$

At infinite dilute condition, when $x_1 \longrightarrow 0$ and $x_2 \longrightarrow 1$, the Eq. 2 will be reduced to $\ln\gamma_1^{\infty}(\text{asym}) \longrightarrow \frac{\alpha_1+\beta_1}{RT}$ for solute species (1). Now after adding and substituting the value of $(\alpha_1 + \beta_1)$ in the expression of $\ln\gamma_1^{\infty}$, one will get $\ln\gamma_1^{\infty}(\text{asym}) = \frac{A_{12}}{RT}$ and hence,

$$A_{12} = RT\ln\gamma_1^{\infty}(\text{asym}). \tag{52}$$

Similarly, when $x_2 \longrightarrow 0$ and $x_1 \longrightarrow 1$, the Eq. 3 will be reduced to $\ln\gamma_2^{\infty}(\text{asym}) = \frac{A_{21}}{RT}$ for the solvent species (2) and therefore,

$$A_{21} = RT\ln\gamma_2^{\infty}(\text{asym}). \tag{53}$$

Therefore, at infinite dilution, one can calculate Margule's parameters from the activity coefficients at infinite dilution from the above two equations. Since, in this article the Margule's parameters are called from the activity coefficient at infinite dilution calculated using COSMOSAC-2013 model, therefore one can write

$$\ln\gamma_1^{\infty}(\text{COSMOSAC}) = \frac{A_{12}}{RT}\,, \tag{54}$$

and

$$\ln\gamma_2^{\infty}(\text{COSMOSAC}) = \frac{A_{21}}{RT}\,. \tag{55}$$

Substituting the value of A_{12} and A_{21} in Eqs 18 and 19, one will get,

$$\ln\gamma_1^{\infty}(\text{asym}) = \ln\gamma_1^{\infty}(\text{COSMOSAC})\,, \tag{56}$$

and

$$\ln\gamma_2^{\infty}(\text{asym}) = \ln\gamma_2^{\infty}(\text{COSMOSAC})\,. \tag{57}$$

Since, we know that

$$\ln\gamma(\text{COSMOSAC}-2013) = \ln\gamma(\text{res}) + \ln\gamma(\text{comb}) + \ln\gamma(\text{dis})\,. \tag{58}$$

Therefore,

$$\ln\gamma(\text{asym}) = \ln\gamma(\text{res}) + \ln\gamma(\text{comb}) + \ln\gamma(\text{dis})\,. \tag{59}$$

Now, our asymmetric model is,

$$\ln\gamma(\text{COSMOSAC}-\text{LANL}) = \ln\gamma(\text{comb}) + \ln\gamma(\text{asym})\,. \tag{60}$$

Substituting $\ln\gamma(\text{asym})$ in the above equation, one will get,

$$\ln\gamma(\text{COSMOSAC}-\text{LANL}) = 2\ln\gamma(\text{comb}) + \ln\gamma(\text{dis}) + \ln\gamma(\text{res})\,. \tag{61}$$

Therefore, subtracting Eq. 59 from Eq. 61, one will get the relationship between the two models which is valid at infinite dilution and that is

$$\ln\gamma(\text{COSMOSAC}-\text{LANL}) - \ln\gamma(\text{COSMOSAC}-2013) = \ln\gamma(\text{comb})\,. \tag{62}$$

References

[1] E. Arslan, R. A. Lalancette and I. Bernal, *Structural Chemistry*, 2017, **28**, 201–212.

[2] A. A. Shinkle, T. J. Pomaville, A. E. S. Sleightholme, L. T. Thompson and C. W. Monroe, *J. Pow. Sour*, 2014, **248**, 1299–1305.

[3] A. A. Shinkle, *Non-Aqueous Single-Metal Redox Flow Batteries*, University of Michigan, 2013.

[4] T. Herr, J. Noack, P. Fischer and J. Tübke, *J. Elect. Acta.*, 2013, **113**, 127–133.

[5] T. Herr, P. Fischer, J. Tübke, K. Pinkwart and P. Elsner, *J. Pow. Sour*, 2014, **265**, 317–324.

[6] M. O. Bamgbopa, N. Pour, Y. Shao-Horn and S. Almheiri, *J. Elect. Acta.*, 2017, **223**, 115–123.

[7] D. Zhang, Q. Liu, X. Shi and Y. Li, *J. Pow. Sour.*, 2012, **203**, 201–205.

[8] A. E. S. Sleightholme, A. A. Shinkle, Q. Liu, Y. Li, C. W. Monroe and L. T. Thompson, *J. Pow. Sour.*, 2011, **196**, 5742–5745.

[9] Q. Liu, A. E. S. Sleightholme, A. A. Shinkle, Y. Li and L. T. Thompson, *J. Elec. Com.*, 2009, **11**, 2312–2315.

[10] A. A. Shinkle, A. E. S. Sleightholme, L. T. Thompson and C. W. Monroe, *J. Appl. Electrochem.*, 2011, **41**, 1191–1199.

[11] A. A. Shinkle, A. E. S. Sleightholme, L. D. Griffith, L. T. Thompson and C. W. Monroe, *J. Pow. Sour.*, 2012, **206**, 490–496.

[12] S.-H. Shin, S.-H. Yun and S.-H. Moon, *RSC Adv.*, 2013, **3**, 9095.

[13] I. L. Escalante-Garcia, J. S. Wainright, L. T. Thompson, and R. F. Savinell, *J. Electrochem. Soc.*, 2015, **162**, A363–A372.

[14] J. F. Kucharyson, L. Cheng, S. O. Tung, L. A. Curtiss and L. T. Thompson, *J. Mat. Chem. A*, 2017, **5**, 13700.

[15] M. Yamagata, N. Tachikawa, Y. Katayama and T. Miura, *Electrochimica Acta*, 2007, **52**, 3317–3322.

[16] N. Tachikawa, Y. Katayama and T. Miura, *Journal of The Electrochemical Society*, 2007, **154 (11)**, F211–F216.

[17] Y. Katayama, R. Fukui and T. Miura, *Journal of The Electrochemical Society*, 2007, **154 (10)**, D534–D537.

[18] N. Tachikawa, Y. Katayama and T. Miura, *Electrochemical and Solid-State Letters*, 2009, **12 (11)**, F39–F41.

[19] Y. Yamato, Y. Katayama and T. Miura, *Journal of The Electrochemical Society*, 2013, **160 (6)**, H309–H314.

[20] Y. Katayama, M. Yoshihara and T. Miura, *Journal of The Electrochemical Society*, 2015, **162 (8)**, H501–H506.

[21] N. Tachikawa, R. Haruyama, K. Yoshii, N. Serizawa and Y. Katayama, *Electrochemistry*, 2018, **86**, 32–34.

[22] M. H. Chakrabarti, F. S. Mjalli, I. M. A. Nashef, M. A. Hashim, M. A. Hussain, L. Bahadori and C. T. J. Low, *Renewable and Sustainable Energy Reviews*, 2014, **30**, 254–270.

[23] M. H. Chakrabarti, N. P. Brandon, F. S. Mjalli, L. Bahadori, I. M. A. Nashef, M. A. Hashim, M. A. Hussain, C. T. J. Low and V. Yufit, *J. Soln. Chem.*, 2013, **42**, 2329–2341.

[24] K. Gong, Q. Fang, S. Gu, S. F. Y. Li and Y. Yan, *Energy Environ. Sci*, 2015, **8**, 3515.

[25] J. M. Prausnitz, R. N. Lichtenthaler and E. G. de Azevedo, *Molecular Thermodynamics of Fluid Phase Equilibria*, Prentice Hall, New York, 3rd edn, 1999.

[26] C. Hansen, *The Three Dimensional Solubility Parameter and Solvent Diffusion Coefficient and Their Importance in Surface Coating Formulation.*, Copenhagen: Danish Technical Press, 1967.

[27] A. Klamt and F. Eckert, *Fluid Phase Equilibria*, 2000, **172**, 43–72.

[28] A. Klamt, *WIRE: Computational Molecular Science*, 2011, **1**, 699–709.

[29] A. Klamt and G. Schüürmann, *J. Chem. Soc. Perkin Trans*, 1993, **2**, 799–805.

[30] S.-T. Lin and S. I. Sandler, *Ind. Eng. Chem. Res.*, 2002, **41**, 899–913.

[31] R. Xiong, S. I. Sandler and R. I. Burnett, *Ind. Eng. Chem. Res.*, 2014, **53**, 8265–8278.

[32] A. Karmakar, R. Mukundan, P. Yang and E. R. Batista, *RSC Advances*, 2019, **9**, 18506–18526.

[33] A. Karmakar, P. Yang and E. R. Batista, *Modelling Solubility of Metal Complexes in Non-Aqueous Media from First Principle Calculations: Application to Redox Flow Cell*, 2018, ISBN: 978-0-8169-1108-0.

[34] A. Karmakar, R. Mukundan, P. Yang and E. R. Batista, *Modeling Solubility of Few Tris Acetylacetonato (acac) Transition Metal Complexes and Their Derivatives in Certain Ionic Liquids from First Principle Molecular Simulation: Application to Redox Flow Cell*, 2019.

[35] R. I. Burnett, *Predicting Liquid-Phase Thermodynamic Properties Using COSMO-SAC*, University of Delaware, 2012.

[36] A. Karmakar, E. R. Batista and P. Yang, ABSTRACTS OF PAPERS OF THE AMERICAN CHEMICAL SOCIETY, United States of America, 2017.

[37] A. Karmakar, E. R. Batista and P. Yang, *Greenhouse Gas Capture : A Recent Theoretical Advancement*, 2018, ISBN: 978-0-8169-1108-0.

[38] A. Karmakar and R. Mukundan, *Phys. Chem. Chem. Phys*, 2019, **21**, 19667–19685.

[39] A. J. Staverman, *Recl. Trav. Chim. Pay-Bas-J. R. Neth. Chem. Soc.*, 1950, **69**, 163–174.

[40] E. A. Guggenheim, *Mixtures: The theory of the equilibrium properties of some simple classes of mixtures, solutions and alloys*, Clarendon Press: Oxford, U.K., 1952.

[41] N. A. Gokcen, *Journal of Phase Equilibria*, 1996, **17**, 50–51.

[42] J. Wisniak, *Chemical Engineering Science*, 1983, **38**, 969.

[43] J. M. Smith, H. C. V. Ness and M. M. Abott, *Introduction to Chemical Engineering Thermodynamics*, McGraw-Hill: New York, 2005.

[44] G. M. Kontogeorgis and G. K. Folas, *Thermodynamic Models for Industrial Applications*, John Wiley & Sons Ltd, United Kingdom, 2010.

[45] *ADF2016, SCM, Theoretical Chemistry, Vrije Universiteit, Amsterdam, The Netherlands, https://www.scm.com.*

[46] J. A. Suttil, J. F. Kucharyson, I. L. Escalante-Garcia, P. J. Cabrera, B. R. James, R. F. Savinell, M. S. Sanford and L. T. Thompson, *J. Mat. Chem. A*, 2015, **3**, 7929.

[47] A. Klamt, V. Jonas, T. Bürgar and J. C. W. Lohrenz, *J. Phys. Chem. A*, 1998, **102**, 5074–5085.

[48] C.-M. Hsieh, S. I. Sandler and S. T. Lin, *Fluid Phase Equilibria*, 2010, **297**, 90–97.

[49] A. Karmakar, M. Duvail, M. Bley, T. Zemb and J.-F. Dufreche, *J. Colsurf A*, 2018, **555**, 713–727.

[50] Z. D. Hill and P. MacCarthy, *J. Chem. Educ.*, 1986, **63(2)**, 162.

[51] J. S. Renny, L. L. Tomasevich, E. H. Tallmadge and D. B. Collum, *Angew. Chem. Int. Ed.*, 2013, **52**, 11998 –12013.

[52] G. Beech and R. M. Lintonbon, *Thermochimica Acta*, 1971, **3 (2)**, 97–105.

[53] T. P. Melia and R. Merrifield, *Journal of Inorganic and Nuclear Chemistry*, 1970, **32 (8)**, 2573–2579.

[54] J. O. M. Bockris and A. K. N. Reddy, *Modern Electrochemistry1: Ionics*, Springer Science+Business Media, LLC, 2nd edn, 1998.

[55] D. S. Abrams and J. M. Prausnitz, *AIChE Journal*, 1975, **21(1)**, 116–128.